AD-A053 297 MASSACHUSETTS INST OF TECH CAMBRIDGE DEPT OF PHYSICS F/G 20/8
A STUDY OF THE REACTION PI(+)P YIELDS DELTA (++)RHO(0), WITH IN--ETC(U)
JUN 77 T F RAMOS

UNCLASSIFIED NL

1 OF 1
AD A053297

END
DATE FILMED
6-78
DDC

A STUDY OF THE REACTION

$$\pi^{+}p \rightarrow \Delta^{++}\rho^{0}$$

WITH INCOMING PION MOMENTUM OF 5.8 GEV/C

by

THOMAS FRANCIS RAMOS
COURSE VIII
JUNE 1977

A STUDY OF THE REACTION

$\pi^+ p \rightarrow \Delta^{++} \rho^0$,

WITH INCOMING PION MOMENTUM OF 5.8 GEV/C

by

THOMAS FRANCIS RAMOS

Submitted to the Department of Physics on May 16, 1977 in partial fulfillment of the requirements for the degree of Master of Science.

ABSTRACT

From a total of 300,000 exposures taken in an experiment using a 30 inch hydrogen bubble chamber at the Argonne National Laboratory, a sample of 2613 events of the type $\pi^+ p \rightarrow p\pi^+\pi^+\pi^-$ were extracted. All of the bubble chamber photographs were measured by the PEPR (Precision Encoding and Pattern Recognition) point guidance system. The data was reduced using the standard TVGP, SQUAW, and ARROW programs.

The sample of four-prong four-constraint events was analyzed under two separate processes, a cluster analysis using the rapidity variable, and a modified Prism Plot analysis using longitudinally Lorentz invariant parameters. Results of the two analyses in obtaining a sample of $\pi^+ p \rightarrow \Delta^{++} \rho^0$ events were compared. Total cross sections for the reactions $\pi^+ p \rightarrow p\pi^+\pi^+\pi^-$ and the partial cross section for the $\Delta^{++}\rho^0$ channel were given.

Comparisons between the Prism Plot data and the predictions of the Dar-Watts-Weisskopf Absorption Model were made. Spin density matrix elements were calculated and studied. The absorption parameters R(s) and d(s) were determined. Evidence that these absorption radii are not independent of the exchange mechanism is introduced.

Thesis Supervisor: Robert I. Hulsizer

Title: Professor of Physics

(1)

(6) A STUDY OF THE REACTION

yields Delta(++) rho(0)

$\pi^{(+)} p \rightarrow \Delta^{++} \rho^{0}$,

WITH INCOMING PION MOMENTUM OF 5.8 GeV/c.

by

(10) THOMAS FRANCIS RAMOS

B.S., UNITED STATES MILITARY ACADEMY

(1969)

(9) Master's thesis,

SUBMITTED IN PARTIAL FULFILLMENT

OF THE REQUIREMENTS FOR THE

DEGREE OF MASTER OF

SCIENCE

at the

MASSACHUSETTS INSTITUTE OF

TECHNOLOGY

(12) 64p.

(11) JUN[redacted]77

Signature of Author [redacted]
Department of Physics, June 1977

Certified by Robert I. Hulsizer
Thesis Supervisor

Accepted by Prof. Fred Koster
Chairman, Departmental Committee
on Graduate Students

461 735

A STUDY OF THE REACTION

$$\pi^+ p \to \Delta^{++} \rho^0,$$

WITH INCOMING PION MOMENTUM OF 5.8 GEV/C

by

THOMAS FRANCIS RAMOS

Submitted to the Department of Physics on May 16, 1977 in partial fulfillment of the requirements for the degree of Master of Science.

ABSTRACT

From a total of 300,000 exposures taken in an experiment using a 30 inch hydrogen bubble chamber at the Argonne National Laboratory, a sample of 2613 events of the type $\pi^+ p \to p\pi^+\pi^+\pi^-$ were extracted, All of the bubble chamber photographs were measured by the PEPR (Precision Encoding and Pattern Recognition) point guidance system. The data was reduced using the standard TVGP, SQUAW, and ARROW programs.

The sample of four-prong four-constraint events was analyzed under two separate processes, a cluster analysis using the rapidity variable, and a modified Prism Plot analysis using longitudinally Lorentz invariant parameters. Results of the two analyses in obtaining a sample of $\pi^+ p \to \Delta^{++} \rho^0$ events were compared. Total cross sections for the reactions $\pi^+ p \to p\pi^+\pi^+\pi^-$ and the partial cross section for the $\Delta^{++}\rho^0$ channel were given.

Comparisons between the Prism Plot data and the predictions of the Dar-Watts-Weisskopf Absorption Model were made. Spin density matrix elements were calculated and studied. The absorption parameters R(s) and d(s) were determined. Evidence that these absorption radii are not independent of the exchange mechanism is introduced.

Thesis Supervisor: Robert I. Hulsizer

Title: Professor of Physics

CONTENTS

ACKNOWLEDGEMENTS

Much of the research that went into this paper would never have been possible without the invaluable help of the physicists in the APC Group of the Laboratory for Nuclear Science. To Professor Irwin Pless I extend my deepest gratitude for introducing me to the group and for reviving my interest in high energy physics. My special thanks goes to Professor Robert Hulsizer, my faculty advisor, for his help and encouragement.

Credit should go to Dr. Michael Hodous, from whom I inherited the 5.8 GeV/c data, and who did the initial data reduction for the experiment.

I would also like to thank my fellow graduate students with APC, especially to Mr. Thomas Lainis and Mr. Jerry P. Silverman for their help and advice with the Prism Plot program and the ABSOR program; to Mr. Austin Napier for his help with the absorption model; and to Mr. James Brau for his many ideas and encouragement during my two years at MIT.

I would like to extend a special word of thanks to Mr. Patrick Miller, whose work with this experiment is mentioned in this paper, and without whose help this paper would never have been possible.

I INTRODUCTION

As a result of many experimental analyses, it has been generally understood that many interactions involving high energy particles that result in a four body final state proceed through quasi two-body intermediate states. For those four-body final state interactions involving a 5.8 GeV/c positive pion striking a proton, the dominant quasi two-body states are that of the $\Delta^{++}\rho^{0}$ channel and nucleonic diffractive dissociation. This thesis discusses separation of the $\Delta^{++}\rho^{0}$ channel and studies the dynamics of this interaction from the point of view of the peripheral model.

The setup for this experiment at the Argonne National Laboratory is described in Section II of this paper. The process of data reduction, from the scanning of the bubble chamber photographs to the production of the data summary tape, is described in Section III. Additionally, total cross sections for the reactions $\pi^{\pm}p \rightarrow p\pi^{\pm}\pi^{+}\pi^{-}$ are given.

There are several models that may be compared with data to learn something about the dynamics of hadron interactions. Applying these models to a sample of events is usually a straightforward matter, but one of the most difficult tasks of the experimental physicist is segregating out the sample of events that belong to the channel appropriate to the model from the many other channels. One method of channel separation is the Prism Plot Analysis, and it is discussed in Section IV. Another method of channel assortment relies on separation the channels by their distribution in the rapidity variable. Although the channel selection process of this method is not quite as clean as that of the Prism Plot, it provides some insight into the kinematics of the four-body state. The rapidity analysis is discussed in Section V.

As stated previously, once a sample of events for a given channel is obtained, it can readily be applied to test the predictions of a theoretical model of the interaction. In this paper, the analysis centers around a Regge pole exchange mechanism with special attention paid to the Peripheral Model. In section VI there is a discussion of the density matrix introduced by J. D. Jackson and K. Gottfried. Additionally, the Dar-Watts-Weisskopf Absorption Model is briefly discussed. In section VII a comparison is made between the data and the predictions of this model.

II EXPERIMENTAL SETUP

A. BACKGROUND

The data used in this paper comes from an experiment done in September 1968, and again in February 1970, at the Argonne National Laboratory's 12.5 GeV/c Zero Gradient Synchrotron (ZGS), where 300,000 exposures were made of a 5.8 GeV/c positive pion beam into the 30 inch Mura Hydrogen Bubble Chamber. The experimental setup has been explained in great detail in several previous papers.[1-3]

B. ZGS 7° BEAM LINE

At intervals of about three times each four seconds, approximately 5% of the primary proton beam in the ZGS was deflected at an angle of 7° to 8°, onto a copper target [See Figure 1]. Each pulse lasted about 100 microseconds. Two quadrupole magnets aligned the beam into a bending magnet that deflected positive particles with a momentum of approximately 5.8 GeV/c through a momentum collimator and a set of electrostatic separators. The beam then went through a second bending magnet and a similar set of electrostatic separators. For the final beam entering the bubble chamber, it was estimated that the proton contamination was less than 0.3%. Kaon, nuon, and positron contamination were limited to 0.7%, 1.3%, and 0.1% respectively. The magnetic field in the bubble chamber was approximately 30 kilogauss.[3]

III DATA REDUCTION

A. INITIAL STEPS

The bubble chamber exposures were scanned on image plane digitizer (IPD) tables. In order to gain reliability in momenta measurements, a fiducial volume was chosen which required all outgoing tracks to be at least 18 centimeters long in order for the event to be accepted. An event occurring within this fiducial volume was marked by a scanner for digital recording at the vertex, along the incoming beam track, and twice along each outgoing track. In the case of the incoming beam track being clustered within 2 mm of another beam track, a separate beam track in the frame, outside the cluster, was measured to determine the incoming beam momentum. This information was punched on cards and fed into a digital computer for recording.

Precise measurement of track parameters was accomplished through use of the PEPR system developed at MIT. Using the guidance input provided by the scanners, PEPR measured and recorded the x and y coordinates of up to twenty points per track to within about 50 mm. This information was recorded for each of the three camera views onto three separate magnetic tapes.[4] The PEPR output was used by a program called TRIMERGE to match the three tracks of each particle and to merge the three separate measurements of PEPR onto a single record.[5]

B. FITTING PROGRAMS

The Three View Geometry Program (TVGP), written at the University of California (Berkely) and modified at the University of Maryland was used to reconstruct the tracks into three dimensional space.[6] The fits done for tracks were obtained by using the proton or pion mass for positive tracks,

and the pion mass for negative tracks.

The three dimensional tracks were kinematically fitted as particles by the SQUAW program, which also originated at the University of California (Berkely), and was modified at the Argonne National Laboratory and the University of Maryland.[7] The incoming pion momentum used to do the kinematical fitting was obtained from a beam map. This was done since momenta measurements based on track curvatures are highly susceptible to error. The beam map was essentially obtained by fitting four-prong events with a four constraint hypothesis, starting with an average value of the beam momentum. Since four prong four-constraint events usually have lower energy outgoing particles, their momenta can be more easily measured. Also, four-prong events with four constraints would provide a relatively better measure of particle momenta than four-prong events with less than four constraints. Those four-prong events that successfully met the four-constraint fit were then used to provide a new average momentum. The process is repeated using the successfully fitted events until the probability distribution of the events is flat.[Fig. 2] The sharp spike near zero occurs since TVGP treats all errors as gaussian distributed when in fact, they are not.

The SQUAW program, with each fit, attempts to minimize a value defined by

$$\chi^2 = \sum_{i,j=1}^{n} (\chi_i^f - \chi_i^m)\, A_{ij} (\chi_i^f - \chi_i^m),$$

where n is the number of variables, χ_i^f is a fitted variable, χ_i^m is the corresponding measured variable, and A_{ij} is an element of the inverse of the error matrix for the measured variables. An acceptable value of χ^2 is usually less than six times the number of constraints in a fit [3].

The SQUAW output carried a maximum of nine hypothetical fits per event. The following table is a listing of events that had more than one successful SQUAW fit:

EVENT TYPE PUT ON DST	ALTERNATE HYPOTHESES ADDED BY SQUAW				
	$\pi^+p\pi^+\pi^-$	$\pi^+p\pi^+\pi^-\pi^0$	$\pi^+p\pi^+\pi^-$ mm (meson)	$\pi^+n\pi^+\pi^+\pi^-$	$\pi^+n\pi^+\pi^+\pi^-$ mm (baryon)
$\pi^+p\pi^+\pi^-$	2613	1199	2459	316	561
$\pi^+p\pi^+\pi^-\pi^0$	40	4529	4463	1142	2647
$\pi^+n\pi^+\pi^+\pi^-$	7	737	1169	1368	1338
$\pi^+p\pi^+\pi^-$ mm (meson)			7509		
$\pi^+n\pi^+\pi^+\pi^-$ mm (baryon)					4056

TABLE 1

Events of the last two types have no other SQUAW fits because hypotheses with zero constraints are the last to be selected onto the data summary tape.

C. SELECTING EVENTS

The SQUAW output was checked by a modified version of the ARROW program called ARROWN. The program selectively rejected events with χ^2 greater than six times their number of constraints. Ionization errors were also checked by ARROWN by use of the variable σ, defined by

$$\sigma = \frac{1}{N-1} \sum_{1}^{N} (\beta^2 - q/\log \ell_1),$$

where N is the number of tracks, β is the usual ratio of the particle velocity to the speed of light, ℓ is the bubble density of the track, and q is varied in order to minimize σ [1,2,3]. Any particle misidentified

by SQUAW would have a discrepancy between its predicted and measured ionizations, causing the minimum value of σ to become greater. As with earlier experiments using the Argonne National Laboratory's bubble chamber, an upper limiting value of .03 was set for σ [8-11]. The ionization of tracks in approximately one hundred events were hand measured and were found to reasonably correlate to the ionization values given by the ARROWN program.

Obvious discrepancies such as an incorrectly identified proton track would also cause ARROWN to reject an event. Events that had more than one successful fit had only the first three fits with the highest number of constraints written onto the Data Summary Tape, the output of ARROWN. For events with more than one successful fit the following format was used: a four constraint fit was chosen over a fit with three constraints, a three constraint fit was chosen over a one constraint fit, and a one constraint fit was preferred over a fit with no constraints.

IV CROSS SECTIONS

A. GENERAL

The pion flux was obtained by taking a track count on every hundredth frame and averaging the count over the entire experiment. It was found that only 65% of the four prong events scanned on the IPD tables were on the DST, where they were lost from system error, failure to make any SQUAW fits, or were rejected by ARROW for failing ionization criteria. Assuming that each four prong channel had an equal probability of losses during reduction, a factor of .65 was used to correct for four prong-4 constraint event losses.

B. VISIBILITY ANGLE

An important source of errors is the misidentification of events by the scanners because one or more particles in the interaction had components of their velocity almost perpendicular to the observation glass of the bubble chamber. Identification prejudices due to this effect can be determined by an analysis of the visibility angle, θ_v, defined as:

$$\cos\theta_v = \frac{(\vec{\pi}_{inc} \times \hat{k}) \cdot (\vec{\pi}_{inc} \times \vec{S})}{|\vec{\pi}_{inc} \times \hat{k}| \quad |\vec{\pi}_{inc} \times \vec{S}|}$$

$\vec{\pi}_{inc}$ is the momentum vector of the incident pion, $\hat{k}$ is a unit vector in the direction of the observation window, and $\vec{S}$ is the momentum vector of the slowest particle in the reaction. An event with $\theta_v = 0^0$ is one in which the slowest particle traveled in the $\hat{k}$ direction. The distribution of θ_v for this experiment is shown in Fig. 3. As can be seen, there is a definite decline in the event count in the regions $14^0 > \theta_v > 166$, for the π^+ events. Since the θ_v distribution should be isotropic, it can be determined that the data lost approximately 4% of its events, necessitating an increase in the number of events by a factor of 1.04.

C. CROSS SECTIONS

The value for the hydrogen density used in the cross section calculations was .0615±.001 gm/cm^3. The length of the fiducial volume used was 26.2±.35 cm. Although this paper is concerned with π^+p interactions, data analysis for an identical experiment involving π^-p interactions was also done. The results are:

$\pi^+p \rightarrow p\pi^+\pi^+\pi^-$: 2613 events or 2.21±.12 mb

$\pi^-p \rightarrow p\pi^+\pi^-\pi^-$: 1856 events or 1.39±.08 mb

Invariant mass distributions for various combinations of the interaction particles in the π^+p reaction are shown in Figs. 4 to 9. As can be seen from Figs. 4 and 5, the Δ^{++} resonance is very pronounced while the A^0 is barely discernible above the background. There are also strong indicators of ρ^0 and f^0 production [Fig.7]. There is also some indication of A meson production, with the strongest enhancement in the A_2 region [Fig. 9].

V PRISM PLOT ANALYSIS

The $\Delta^{++}\rho^0$ channel analysis in this paper was based on events channeled by a variation of the Prism Plot Analysis done by Patrick A. Miller, a graduate student with the Laboratory for Nuclear Science [18]. The Prism Plot Analysis involves the procedure of sorting out the various intermediate states that lead to the final state seen in the bubble chamber, such as $\pi^+ p \to p\pi^+\pi^+\pi^-$. In the Miller version, the ordinary prism plot coordinates were replaced with a set of longitudinally Lorentz invariant variables.

These variables are composed of the energy, E, and longitudinal momentum, p_L. The Lorentz transformation for these variables is

$$E_i' + p_{Li}' = K(E_i + p_{Li}), \quad i=1,2,3,4$$

where $K = \sqrt{(1-\beta)/(1+\beta)}$, and $\beta = v/c$.

Then we see that the quantities $q^{\pm}$ are Lorentz invariant where,

$$q^{\pm}_i = \frac{E_i \pm p_{Li}}{(E + p_L)_{Tot}}.$$

It is found that particles arising from different intermediate states will tend to occupy different regions of phase space. This is in fact the case, although the regions occupied by the various intermediate states overlap [19,20,21]. Briefly, the Prism Plot Analysis plots real events into a 3N-5 dimensional kinematic space; N being the number of particles in the final state. For each intermediate state it then produces a large number of events having general kinematical properties of that particular channel, and plots them together with the real events. The plotted space is broken up into arbitrarily small boxes. Each real event is then given

a probability weight for each channel based on the number and type of generated events that occupy the box it is in. These so-called 'tagged' real events then provide a production angular distribution for each channel which is used to generate events again, and the process is repeated. This iterative process continues until the distribution of events in each channel reaches a constant form, which usually occurs after ten to twenty iterations. When the analysis is finished, each event carries a weight for belonging to each intermediate state. The sum of all weights for a channel then gives the total number of events in the channel [3]. Of the 2613 four prong-four constraint events on the DST, Mr. Miller's Prism Plot Analysis found 876 events to be in the channel $\pi^+ p \rightarrow \Delta^{++}\rho^0$, giving a partial cross section for this channel of .740 ± .090 mb. Figure 10 shows the invariant mass distributions of the $p\pi^+$ and the $\pi^+\pi^-$ sorted out by this process.

VI RAPIDITY ANALYSIS

A. RAPIDITY

If a pion strikes a proton in a bubble chamber and interacts to form one or more resonances, we would expect to find the decay products emerge from the interaction in clusters of particles corresponding to the respective resonances. One method of analysing the clustering of particles is by means of their longitudinal velocity. This is because particles of a cluster, except for differential velocity acquired in the decay process, would have the same velocity as the entire cluster in the limit where the sum of the particle masses is the cluster mass. An ideal variable for this purpose is rapidity, usually labelled y, defined as

$$y = \frac{1}{2} \ln\left|[E+p]/[E-p]\right| = \frac{1}{2} \ln\left|[1+\beta]/[1-\beta]\right|$$

where E, p, and β are the particle's energy, longitudinal momentum, and longitudinal velocity ratio respectively. Rapidity suits our purposes well here since the momentum of a particle is proportional to its mass. Rapidity has the Lorentz invariant property,

$$dy = dp/dE.$$

It therefore transforms like a Galilean velocity. In other words, a rapidity distribution will have the same shape in any Lorentz frame along the longitudinal axis.

B. CLUSTER DEFINITIONS

There are two general ways of defining clusters based on rapidity [12, 13,14]. Since this paper is concerned with only the $\Delta^{++}\rho^0$ channel, only intermediate states having two clusters were considered. In method one, all the final state particles are combined in every possible combination that

will provide two clusters. The rapidity of one hypothetical cluster is compared with its corresponding partner. That combination that provides the largest gap in rapidity between the clusters defines the two clusters for a given event. In method two, the particles are ordered with respect to their rapidities and the rapidity gap between each set of two particles is measured. Particles on either side of the largest gap are then defined as composing the two clusters. In the following sections only clusters arrived at by method two will be used. To clarify terminology, a two by two cluster grouping represents an event with the gap between the second and third particle, while a one by three grouping is one with the gap between the first and second particles or the third and fourth particles. Cluster distributions based on the two methods discussed above do not differ greatly. The distributions are shown in the table below:

		CLUSTER B				
		$\pi^+\pi^+\pi^-$	$p\pi^+\pi^-$	$p\pi^+\pi^+$	$\pi^+\pi^-$	$p\pi^+$
	p	364 (226)				
	π^+		1130 (1338)			
CLUSTER A	π^-			481 (575)		
	$p\pi^+$				515 (369)	
	$p\pi^-$					123 (111)

METHOD 2
(METHOD 1)

TABLE 2

To test whether the clusters defined above actually show signs of intermediate state resonances we can look at the invariant mass plots of the 2x2 clusters. The $p\pi^+$ and $\pi^+\pi^-$ clusterings should be dominated by Δ^{++} and ρ^0. Method 2 provides a larger sampling of events in these groupings, and when looking at the invariant mass plots (See Fig. 11) of these groupings we see that they are indeed dominated by the Δ^{++} and ρ^0 resonances.

The question should arise that if the Prism Plot Analysis discussed in Section V provides relatively clean samples of the various channels, than why discuss a rapidity analysis? The answer is that for a three body final state, each iteration of the analysis can take an IBM 360 Computer up to 2 hours to run. The time is longer for higher multiplicity states. Additionally, tagging routines for multiplicity states of the order of six or above have yet to be developed. For practical reasons then, i.e., lack of time or funds, it may not be feasible to complete a prism plot analysis for a set of data. It is the purpose of this section to demonstrate that a reasonably clean sample can be obtained through rapidity analysis. In a later section we will see that there is reasonable agreement between clustered and tagged events when their mass distributions are compared.

C. THE $\Delta^{++}\rho^0$ SAMPLE

Figures 12a through d show the rapidity distributions in the CM frame, for each of the final state particles in all the four prong-four constraint events. It is easily seen that the leading positive pion, defined as the pion with the greater longitudinal velocity, invariably emerges in the forward direction while the proton invariably emerges in the backward direction. However, fully 4/5 of the slower positive pions lie in the negative rapidity region while only about 1/2 of the negative pions lie in the positive rapidity region. A study of these four distributions can

reveal several features of the interaction. Because of the greater number of particles with negative rapidity one could properly surmise that the amplitude of nucleonic diffractive dissociation (DD) is greater than that for pion diffractive dissociation. It is also apparent that the Δ^{++} resonance events outnumber the Δ^{0} events. The prism plot analysis confirms these hypotheses. In any case, the Δ^{++} can come from a proton (DD) channel as well as the $\Delta^{++}\rho^{0}$ channel, and the ρ^{0} may also come from A meson decay. It is one's major task then to isolate events that give rise to these resonances into their proper channels.

From kinematical considerations, we would expect that quasi-two body intermediate states, in which both intermediate particles themselves decay into two particles, would provide most of the events in the two by two particle cluster groupings. By a previous argument we would expect the $\Delta^{0}\rho^{+}$ sample to be small. Therefore, we would expect to see ρ^{0} and f^{0} mesons in the $\pi^{+}\pi^{-}$ invariant mass of the 2 x 2 group. As shown in Figure 11, there is indeed a ρ^{0} enhancement but very little if any f meson. This can be explained by the fact that because of the great mass of the f^{0}, the decaying pions will carry much greater kinetic energy. Since the f^{0} decays with an angular distribution proportional to $\cos^{2}\theta$, where θ is the polar angle in the Gottfried-Jackson frame of the f^{0}, we would expect a majority of the decaying pions to have either extremely high or low longitudinal momenta, with a correspondingly large difference in their rapidities, say on the order of 2.0. Because their momenta are relatively much greater than those of the pions from ρ^{0} decay, the rapidity of the backward pion is closer to the rapidities of the Δ^{++} decay products than to its sister pion. In a rapidity analysis it would then show up as a three by one cluster group.

We now have a fairly clean sample of 448 $\Delta^{++}\rho^0$ events. Where are the other 450 events discovered in the Prism Plot Analysis? Let's look at the ρ^0 in its rest frame and define the polar axis as the direction of the incoming beam.

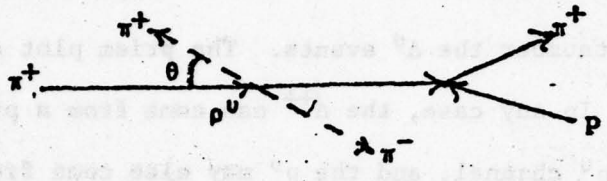

The rapidity of the ρ^0 is greater than that of the Δ^{++} since the ρ^0 emerges from the beam pion vertex while the Δ^{++} emerges from the proton vertex. (Fig. 14) Therefore, pions decaying from the ρ^0 should have a rapidity greater than either of the decay products of the Δ^{++}, and we would see a two by two clustering. Figure 13 shows the distribution of cos θ for this group, and we see that it contains a higher proportion of events with $\pi/4<\theta<3\pi/4$. The missing events then are those with small θ, which show up as a three by one clustering.

There are three types of three by one cluster groupings, and they can be defined by their respective one particle clusters. The three types then are the proton alone, negative pion alone, and positive pion alone. As might be expected, the proton alone groupings show A meson production and very little of anything else.(Fig. 15) It now remains to analyze the other two types.

D. π^- CLUSTER GROUPING

It turns out that the π^- cluster grouping provides a rich sample of $\Delta^{++}\rho^0$ channel events.(Fig. 16) Clearly, this cluster grouping represents events in which the vector meson of the upper vertex decayed with a negative pion in forward direction. If we compare these data with the π^+ cluster

grouping mass plots (Fig. 17), we see that the $^-$ grouping is relatively cleaner. This is to be expected since there are more channels that can possibly compete in events with the π^+ alone.

There remains the matter of separating the f^0 from the ρ^0 events. A mass cut can be used to accomplish this, but a slightly cleaner cut can be obtained by making a rapidity cut. This is done by plotting the rapidities of $\pi^+\pi^-$ systems that make up the mesons (Fig. 18). Since the ρ^0 is the lighter of the two mesons its rapidity will be greater, with a lower edge about the value .7 (see Fig. 14). Figure 19 shows the invariant masses of the $\pi^+\pi^-$ and $p\pi^+$ systems after this cut.

E. π^+ CLUSTER GROUPING

As shown in Fig. 16, the $\Delta^{++}\rho^0$ channel clearly dominates the π^- alone cluster grouping. However, a look at Fig. 17 will show that this is not the case with the π^+ alone cluster grouping. The nucleonic DD channel especially, shares this cluster grouping. Now in reality, the $\Delta^{++}\rho^0$ channel is a 2x2 cluster grouping and proton DD is a 3x1 cluster grouping, so we might suspect that 3x1 cluster groupings in which the three particle width is greater than the cluster gap itself might indeed be a 2x2 cluster grouping. Therefore, events were selected that either had a three particle rapidity width greater than the cluster gap, or had a cluster gap less than 1.0 in rapidity.

The invariant mass distributions for the total selected events are shown in Figure 20. One sees that the cut sample is indeed a fairly rich source of $\Delta^{++}\rho^0$ events. With this final cut, a sample of about 800 events had been accumulated for further study.

VII THE ONE PARTICLE EXCHANGE PROCESS

A. THE PERIPHERAL MODEL

An examination of the rapidity distributions of the Δ^{++} and ρ^0 in Figure 14, shows that in these interactions [in the center of mass frame], the meson predominantly scatters forward and the baryon scatters backward. Observations of many other types of inelastic interactions has shown that it is generally true that the secondary particles will form two clusters of particles, associated with the primary beam and target particles. This observation, plus the indications that many inelastic reactions proceed via intermediate states, has led to the development of the peripheral model for strong interactions.

The model proposes that the interaction particles do not collide head on, but glance at each other without significantly changing their directions. The model would say that the incoming pion interacts with the pion cloud surrounding the proton, rather than with the proton itself. The interaction is said to be dominated by the exchange of a virtual particle, and can be depicted by the Feynman diagram shown below.

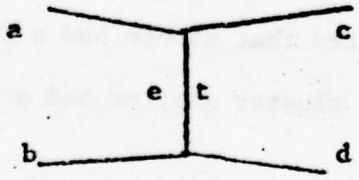

Here, a and b are the incoming and target particles respectively, c and d are the intermediate resonances of the upper and lower vertices, e is the exchange particle and t is the four-momentum transfer.

B. THE EXCHANGE PARTICLE

For the particular case under study here a is the beam pion, b is the proton target, c the rho meson, and d is the delta baryon. The quantum numbers of the exchange particle can be deduced from conservation laws. Since the G-parity of a pion is negative and the G-parity of the rho is positive, the exchange particle must have a negative G-parity. Its charm and strangeness are zero since neither the pion nor the rho are charmed or strange particles. Conservation of Isospin requires the exchange particle to have an isospin of 0,1 at the upper vertex, and an isospin of 1,2 at the lower vertex, therefore, we see its isospin is 1. A quick look in the the Rosenfeld Tables will show that only pions and the A_2 meson meet these requirements.

The peripheral model deals with long range forces as for example the form of the Yukawa potential, $\exp(-mr/r)$, where the range of the force is inversely proportional to the mass of the exchange particle. We might suspect then that the lighter pion would be the primary exchange particle, and indeed, as we will see in the data, it does dominate the exchange process.

C. DENSITY MATRIX ELEMENTS

The decay angular distributions used in this study were derived by Pilkuhn, et. al.[15]. For a resonance with J=1,

$$W(\cos\theta,\phi) = \frac{3}{4}\pi\{\frac{1}{2}(1-\rho_{00}) + \frac{1}{2}(3\rho_{00}-1)\cos^2\theta - \rho_{1,-1}\sin^2\theta\cos2\phi - \sqrt{2}\,\mathrm{Re}\rho_{1,0}\sin2\theta\cos\phi\}.$$

For a resonance with J=3/2,

$$W(\cos\theta,\phi) = \frac{3}{4}\pi\{\frac{1}{6}(1+4\rho_{33}) + \frac{1}{2}(1-4\rho_{33})\cos^2\theta - \frac{2}{\sqrt{3}}\mathrm{Re}\rho_{3,-1}\sin^2\theta\cos2\phi - \frac{2}{\sqrt{3}}\mathrm{Re}\rho_{31}\sin2\theta\cos\phi\}.$$

In these equations, $\rho_{\mu\nu}$ represents the density matrix element. Let $|u\rangle$ be the pure spin states which contribute with weights q_u to the quantum mechanical mixture of a resonance. ρ is defined then by

$$\rho = \Sigma_u |u\rangle q_u \langle u| \quad \text{with} \quad \Sigma_u q_u = 1.$$

The subscripts of ρ refer to the (2J+1) eigenstates of the Z components of the spin operator of the resonance. $\rho_{\mu\nu}$ is then a (2J+1) dimensional matrix with the elements

$$\rho_{\mu\nu} = \langle\mu|\rho|\nu\rangle = \Sigma_u \langle\mu|u\rangle p_u \langle u|\nu\rangle .$$

We see then that $\rho_{\mu\nu}$ is the weight with which the state $|m\rangle$ is contained in the mixture. A derivation of the density matrix is given in a paper by J. D. Jackson, et. al.[15] and an elegant explanation of the properties of density matrices are given in a lecture by N. Schmitz and M. Pilkuhn [16]. Our purpose here is to understand the basic properties of the components of the density matrix and their use in understanding the dynamics of high energy interactions.

The density matrix has two general properties pertinent to this investigation. The first property is that the density matrix is normalized, that is,

$$\Sigma_\mu \rho_{\mu\mu} = \mathrm{Tr}\,\rho = 1 .$$

A second property stems from conservation of parity. For an unpolarized incident beam

$$\rho_{\mu\nu} = (-1)^{\mu-\nu} .$$

This property holds because the matrix is Hermitian.[17] This relation is equivalent to stating that

$$\rho_{\mu\mu} = \rho_{-\mu-\mu} .$$

D. PREDICTIONS OF THE ONE MESON EXCHANGE (OME) MODEL BASED ON DENSITY MATRICES.

Consider the production of the rho meson at the upper vertex of the diagram drawn in Section A. The process can be shown schematically in the diagram below, with the particles shown in the form (J^P)

Earlier it was shown that only two mesons could be the exchange particle in order to conserve parity, angular momentum and isospin, and these were the pion and the A_2 meson. Let's check how these mesons will affect the density matrix.

Case of 2^+ exchange particle (A_2)

From conservation of angular momentum, L=1,2,3 and L_z=0. Parity conservation requires L to be even. Conservation of L_z gives $J_{z_{A_2}}$=0,$\pm$ 1. From the definition of the density matrix

$$\rho_{\mu\mu} = \Sigma_u \langle u|\mu\rangle^2 p_u .$$

The Clebsch-Gordon coefficients for these calculations gives the values $\rho_{0_\mu} = \rho_{\mu 0} = 0$. Again, using the normalization condition,

$$\rho_{11} = \frac{1}{2}(1-\rho_{00}) .$$

$$\rho_{11} = \frac{1}{2}$$

The value of ρ_{1-1} is arbitrary.

Case of 0^- exchange particle (π^+)

From conservation of angular momentum, L=1 and L_z=0, therefore,

parity is also conserved since,

$$P(\pi^+)\ P(\pi^+)\ (-1)^L = P(\rho^0) = -1.$$

Conservation of the z component of angular momentum will allow only m states equal to zero, that is,

$$|m> = |\pm 1> \text{ are not allowed.}$$

Therefore,

$$\rho_{\pm 1,m} = \rho_{m,\pm 1} = 0.$$

Since the trace of the density matrix must equal unity, it follows that,

$$\rho_{00} = 1.$$

Case for the Lower Vertex.

As a final calculation we can determine the values of the density matrix elements for the lower vertex. The schematic diagram for the reaction would appear as follows:

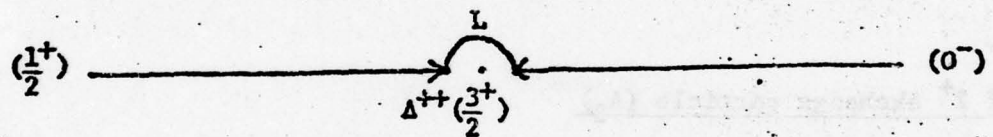

Since the proton has spin 1/2, predictions for the density matrix elements can be made uniquely only for the case of a spinless exchange particle. Therefore, only the case of the pion exchange will be considered. Conservation of angular momentum gives L=1,2 and L_z=0. Parity conservation requires L to be odd. Conservation of L_z requires m=±1/2, which equals the z component of the proton's spin.

$$\rho_{m\pm 3} = \rho_{\pm 3,m} = \sum_{u=-1/2}^{1/2} <\pm 3/2|u>^2\ p_u = 0.$$

(The subscripts have been multiplied by two to simplify notation). Again, from the normalization condition,

$$\rho_{11} = \frac{1}{2}(1-\rho_{33})$$

$$\rho_{11} = \frac{1}{2}.$$

VIII. THE ABSORPTION MODEL OF DAR-WATTS-WEISSKOPF

A. AN ABSORPTIVE MODEL

Figure 22 shows that the cross section of the reaction $\pi^+p \to \Delta^{++}\rho^0$ becomes strongly attenuated for larger values of t, the momentum exchange. As explained earlier, the Peripheral model suggests the mechanism for this reaction is pion exchange with the beam particle glancing past the peripherality of the target. However, the model does not suggest a strong dependency upon t, and therefore fails to explain the strong attenuation in cross section as t increases. Attempts to fit this phenomenon by using form factors have proven unfruitful [25]. However, fairly good fits for the cross section dependence upon t have been given by an idea generally known as the absorption model [15]. Qualitatively, the absorption model states that for higher energy inelastic collisions, there are many channels which the colliding particles can follow. These channels compete with each other, and specifically, cause the cross section of the $\Delta^{++}\rho^0$ channel to be reduced. Since t is inversely proportional to the impact parameter, b, we again see from figure 22 that the absorption effect becomes stronger for smaller b. Now b is related to angular momentum j by the relation,

$$\hbar^2 j(j+1) = (pb)^2.$$

We would expect then that mainly partial waves with small orbital angular momenta would feel the effects of absorption most strongly [16].

We see then that the density matrix elements that were calculated in the previous section must take account of the t dependence of the cross section. This is so because larger production angles will correspond to larger t.

B. A NEW ABSORPTION MODEL FOR HADRON COLLISIONS

The differential cross section for a two-body reaction

$$a + b \to c + d ,$$

with unpolarized incident beam is given by

$$\frac{d\sigma}{dt} = \frac{1}{64sk^2} \frac{1}{(2s_a+1)(2s_b+1)} \sum_{\lambda} |\langle \lambda_a \lambda_b | M | \lambda_c \lambda_d \rangle|^2$$

where s_i, λ_i are the spin and helicity of particle i, s and k are the square of the c.m. energy and the beam momentum respectively, and M is the scattering amplitude matrix [22]. For large enough values of the impact parameter, $M_{[\lambda]}$ can be approximated by an expression obtained from the Born approximation [see Section 4, reference 22]:

$$M_{[\lambda]}(b) = B_{[\lambda]}(b).$$

For smaller impact parameters, in the region where b is smaller than the target radius R, the above relation is no longer true because of suppression by competing channels, and

$$M_{[\lambda]}(b) \ll B_{[\lambda]}(b) \qquad \text{for } b \ll R.$$

To account for the decrease in the matrix amplitude a factor is introduced such that,

$$M_{[\lambda]}(b) = \eta(b)\, B_{[\lambda]}(b),$$

where η has the form

$$\eta(b) = \frac{1}{1+\exp[(R-b)/d]} .$$

Here R and d are the target radius and width respectively, which are assumed to be constant for all channels [22]. Up to now, we have seen a description of the absorption model as given by Dar, Jackson and Gottfried [23,24]. The model of A. Dar, T.L. Watts, and V. Weisskopf modifies this concept by

allowing R and d to be functions of s, the squared c.m. energy. Their new assumption is that the radius R(s) and the width d(s) are slowly increasing functions of s. R(s) takes the form,

$$R(s) \geq \frac{1}{m_1} \log \frac{s}{s_0},$$

m_1 was determined experimentally to be, $m_1 = 0.73$GeV. R(s) is given in units of fermis with $\hbar=c=1$, and d(s) takes on a similar relation, being linearly dependent upon log s [22]. This relationship is suggested for two reasons. Firstly, at higher energies more competing channels are open, and their influence reduces the amplitude. Secondly, the exchange amplitude for mesons that are as yet unknown may become important at higher energies.

With these assumptions then the absorption model makes predictions for $d\sigma/dt$ based on the two parameters R(s) and d(s).

C. COMPARISON WITH EXPERIMENTAL DATA

Figure 22 shows a plot of the experimental $d\sigma/dt$ compared with the model prediction. Figures 23 to 25 show plots of the various density matrix elements with their corresponding theoretical predictions. The theoretical calculations were done with the help of a FORTRAN program called ABSOR developed by T.L. Watts and associates at MIT. Coupling constants for the upper and lower vertices were needed for the calculations. They were obtained by using the relations

$$\Gamma_{\rho\upsilon} = \frac{2}{3} \frac{g^2}{4\pi} \frac{p^3}{M^2} \qquad [26]$$

$$\Gamma_{\Delta++} = \frac{1}{6} \frac{G^2}{4\pi} \frac{p^3[(M+m_p)^2 - m_\pi^2]}{m_e^2}$$

In these equations, p is the decay momentum of the decay particles in the resonance rest frame and Γ is the full width. The values for the coupling constants were found to be,

$$g^2/4\pi = 2.69, \text{ upper vertex,}$$

$$G^2/4\pi = 0.279, \text{ lower vertex.}$$

The values for R(s) and d(s), using events obtained through the Prism Plot analysis, were determined by taking those parameters that gave a least chi squared fit between the experimental and theoretical distributions of $d\sigma/dt$. With $s=11.78$ GeV^2, they were found to be:

$$R = 1.042 \pm .012 \text{ fermi}$$

$$d = 0.040 \pm .02 \text{ fermi.}$$

Values for R(s) and d(s) were additionally obtained by using events from the rapidity analysis discussed earlier and finally, from a sample of events obtained by making simultaneous mass cuts for the Δ^{++} and ρ^0 resonances. The final values for the cluster analysis events were determined to be:

$$R = 1.11 \pm .02 \text{ fermi}$$

$$d = 0.03 \pm .02 \text{ fermi.}$$

For the mass cut events the results were:

$$R = 1.03 \pm .02 \text{ fermi}$$

$$d = 0.03 \pm .02 \text{ fermi.}$$

CONCLUSIONS.

A graphical comparison between the theoretical predictions for R and d and the values calculated from the Prism Plot events is shown in Figure 26. As can be seen, the theoretical predictions for R and d

are 0.9 fermi and 0.12 fermi respectively. The most reasonable explanation for this discrepency between the calculated and predicted values may be an assumption made in the model that R and d are independent of the type of exchange particle involved in the interaction. The linear theoretical projections for R and d shown in Figure 26 had been arrived at by fitting the calculated values from the interaction,

$$\pi^- p \rightarrow \pi^0 n,$$

at several different energies. This reaction involves ρ^- exchange. It would seem likely then, from the data shown here, that the absorption radii for ρ exchange may not necessarily be the same as the radii for interactions with other exchange particles.

To follow up on this conjecture a similar analysis was done on data using a pion beam of 3.9 GeV/c. The partial cross section for the $\Delta^{++}\rho^0$ channel at this momentum was determined to be $1.50 \pm .04$ mb[29]. By the methods described above the following values were obtained:

$$R = .985 \pm .007f$$

$$d = .08 \pm .02f$$

These values are also shown plotted on Figure 26. Since the differential cross section is very insensitive to changes in d, little can be said here about the behavior of d for different values of the cm energy. However, the values of R do seem to be consistantly high compared to the predicted values of R. Many more experimental points will be needed of course, but there is a good possibility that R values in pion exchange reactions are also linearly proportional to log s, but larger than the R values for corresponding values of s, for the ρ meson exchange process.

In any case, it is obvious that the Dar-Watts-Weisskopf Absorption Model provides an excellent interpretation for the data presented here. It should be noted here also that the fitted t distribution for the Prism Plot sample provided a minimum chi squared approximately one third as large as either the cluster analysis sample or the mass cut sample. It seems likely that absorption radii are larger for pion exchange reactions than for rho meson exchange processes, however, further investigation is needed to find out more quantitatively how the absorption radii behave for various values of the cm energy.

REFERENCES

(1) A. Sheng, "An Analysis of the Reaction $\pi^+ p \to p\pi^+\pi^+\pi^-$ at 5.72 GeV/c", Ph.D. Thesis, MIT, 1970 (unpublished)

(2) F.T.Dao, "An Analysis of the Reaction $\pi^+ p \to p\pi^+\pi^+\pi^-\pi^0$ at 5.72 GeV/c", Ph.D. Thesis, MIT, 1970 (unpublished)

(3) M.F.Hodous, "A Cross Channel Isospin Analysis of Pion-Induced Three-Particle States at 5.8 GeV/c Incident Pion Momentum", Ph.D. Thesis, MIT, 1976 (unpublished)

(4) P.L.Bastien, et. al., "The PEPR Programming System", Methods of Computational Physics, Vol 5, Academic Press, New York (1966)

(5) P.L.Bastien, J.N.Snyder, and V.Pless, Computer Physics Communications, Vol 2, 394 (1971)

(6) F.T.Solmitz, et. al., Alvarez Programmer's Note P-117, 2d Ed (1966)

(7) O.I.Dahl,et.al., Alvarez Programmer's Note P-126, (1965)

(8) R.A.Singer, Ph.D. Thesis, MIT, 1972 (unpublished)

(9) L.D.Kirkpatrick, Ph.D. Thesis, MIT, 1968 (unpublished)

(10) F.C.Winkelman, Ph.D. Thesis, MIT, 1968 (unpublished)

(11) J.Wolfson, Ph.D. Thesis, MIT, 1968 (unpublished)

(12) W.Burdett,et.al., Nucl. Phys. B48, 13 (1972)

(13) V.P.Kenney,et.al., "Leading Particles and Leading Clusters in $\pi^- p$ Single Particle Inclusive Reactions at 200 GeV/c",(unpublished)

(14) H.Boettcher,et.al., Nucl. Phys. B81, 365 (1974)

(15) J.D.Jackson and H.Pilkuhn, Nuovo Cimento 33, 906 (1964)

(16) N.Schmitz and H.Pilkuhn, "Peripheral Collisions and the Peripheral Model", Proceedings of the CERN 1965 Easter School for Physicists, Vol 1, 1965

(17) B.Feld, Models of Elementary Particles, Blaisdell Publishing Co., New York, 1969, p.123

(18) P.Miller, Ph.D. Thesis, MIT, 1977 (unpublished)

(19) L.Van Hove, Nucl. Phys. B9, 331 (1969)

(20) J.Brau, et.al., Phys. Rev. Ltrs. 27, 1481 (1971)

(21) H.Haber, "Prism Plot Analysis of the Five Body Final State", M.S. Thesis, MIT, 1973 (unpublished)

(22) A.Dar, T.L.Watts and V.Weisskopf, Nucl. Phys. B13, 477 (1969)

(23) K.Gottfried and J.D.Jackson, Nuovo Cimento 34, 735 (1965)

(24) A.Dar and W.Tobocman, Phys. Rev. Ltrs. 12, 511 (1964)

(25) K.Gottfried and J.D.Jackson, Nuovo Cimento 33, 916 (1964)

(26) J.J.Sakurai, Phys. Rev. Ltrs. 17, 1021 (1966)

(27) H.Pilkuhn, "The Peripheral Model", Methods in Subatomic Physics, Vol 1, M.Nikolic, ed., Gordon and Breach Inc., New York, 1968

(28) E.Bracci, et.al., Compilation of Cross Sections, Vol 1, CERN and Lawrence Berkeley Laboratory, 1972

(29) B.Haber, et.al., Phys. Rev. D11, 495 (1975)

FIGURES

1) EXPERIMENTAL SETUP AT ARGONNE NATIONAL LABORATORY'S ZGS

2) PROBABILITY DISTRIBUTION OF DATA

3) VISIBILITY ANGLE DISTRIBUTION

4) INVARIANT MASS OF $p\pi^+$

5) INVARIANT MASS OF $p\pi^-$

6) INVARIANT MASS OF $\pi^+\pi^+$

7) INVARIANT MASS OF $\pi^+\pi^-$

8) INVARIANT MASS OF $p\pi^+\pi^-$

9) INVARIANT MASS OF $\pi^+\pi^+\pi^-$

10) INVARIANT MASS OF $p\pi^+$ AND $\pi^+\pi^-$ OF PRISM PLOT DATA

11) INVARIANT MASS OF $p\pi^+$ AND $\pi^+\pi^-$ OF EVENTS IN 2X2 CLUSTER GROUPINGS

12) RAPIDITY DISTRIBUTIONS OF p, $\pi^+(f)$, $\pi^+(s)$, AND π^- IN CM FRAME

13) ANGULAR DISTRIBUTION OF ρ^0 IN 2X2 CLUSTER GROUPINGS

14) RAPIDITIES OF Δ^{++} AND ρ^0 USING PRISM PLOT DATA

15) INVARIANT MASS OF $p\pi^+$, $\pi^+\pi^-$, AND $\pi^+\pi^+\pi^-$ IN THE p ALONE CLUSTER GROUPINGS

16) INVARIANT MASS OF $p\pi^+$ AND $\pi^+\pi^-$ IN THE π^- ALONE CLUSTER GROUPINGS

17) INVARIANT MASS OF $p\pi^+$, $\pi^+\pi^-$, AND $\pi^+\pi^+\pi^-$ IN THE π^+ ALONE CLUSTER GROUPINGS

18) RAPIDITY OF $\pi^+\pi^-$ SYSTEM IN THE π^- ALONE CLUSTER GROUPINGS

19) INVARIANT MASS OF $\pi^+\pi^-$ AND $p\pi^+$ AFTER RAPIDITY CUT

20) INVARIANT MASS OF $p\pi^+$ AND $\pi^+\pi^-$ AFTER TOTAL CLUSTER ANALYSIS

21) t' DISTRIBUTION FOR PRISM PLOT DATA

22) t' DISTRIBUTIONS FOR PRISM PLOT DATA AND ABSORPTION MODEL

23) DENSITY MATRIX ELEMENTS ρ_{00} AND Re ρ_{10}

24) DENSITY MATRIX ELEMENTS ρ_{1-1} AND ρ_{33}

25) DENSITY MATRIX ELEMENTS ρ_{31} AND ρ_{3-1}

26) R[S] AND D[S]

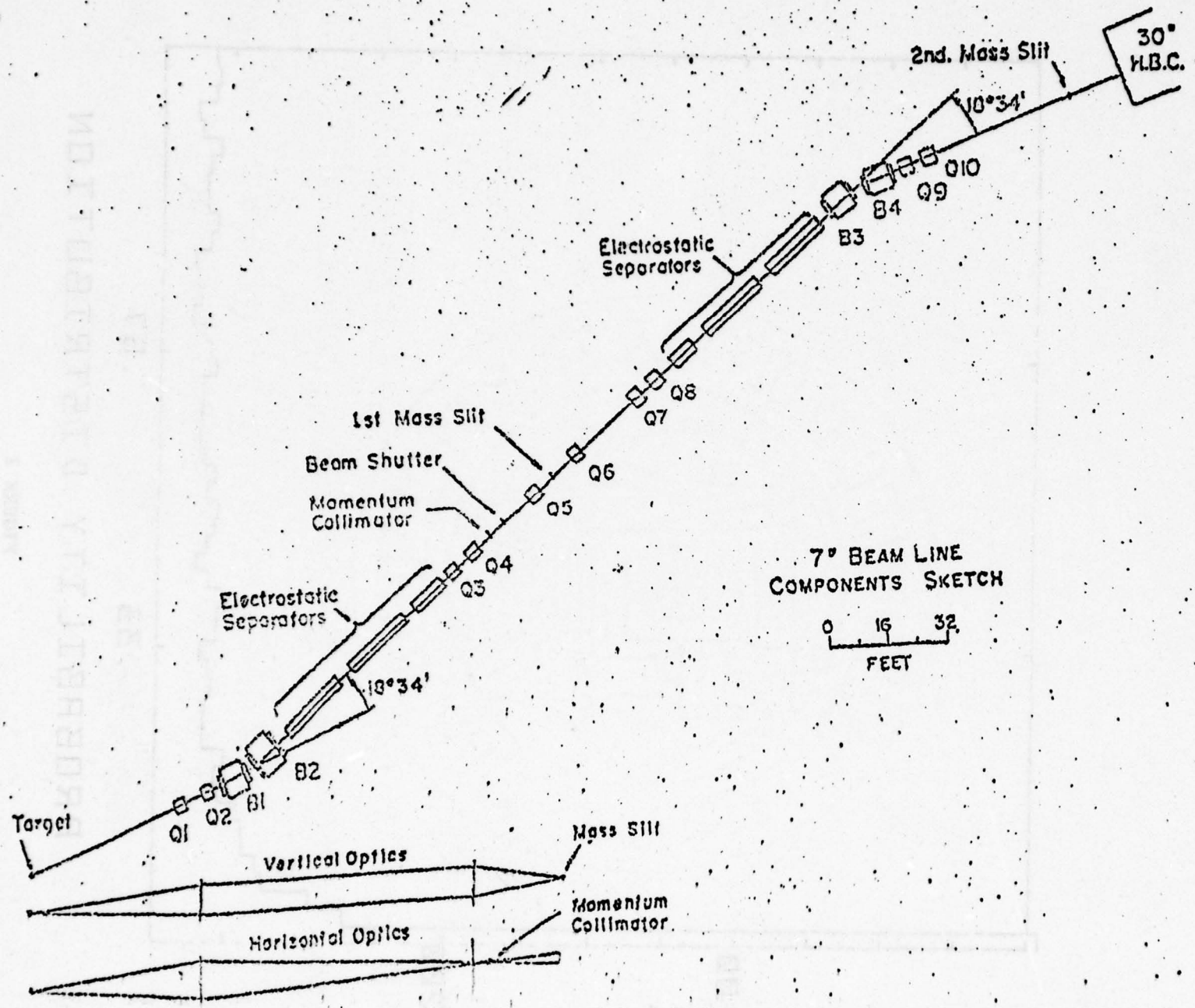
30°
H.B.C.
2nd. Mass Slit
10°34'
Q10
Q9
B4
B3
Electrostatic
Separators
Q8
Q7
Q6
1st Mass Slit
Beam Shutter
Momentum
Collimator
Q5
Q4
Q3
Electrostatic
Separators
18°34'
B2
B1
Q2
Q1
Target
7° BEAM LINE
COMPONENTS SKETCH
0 16 32
FEET
Mass Slit
Vertical Optics
Momentum
Collimator
Horizontal Optics

Figure 1

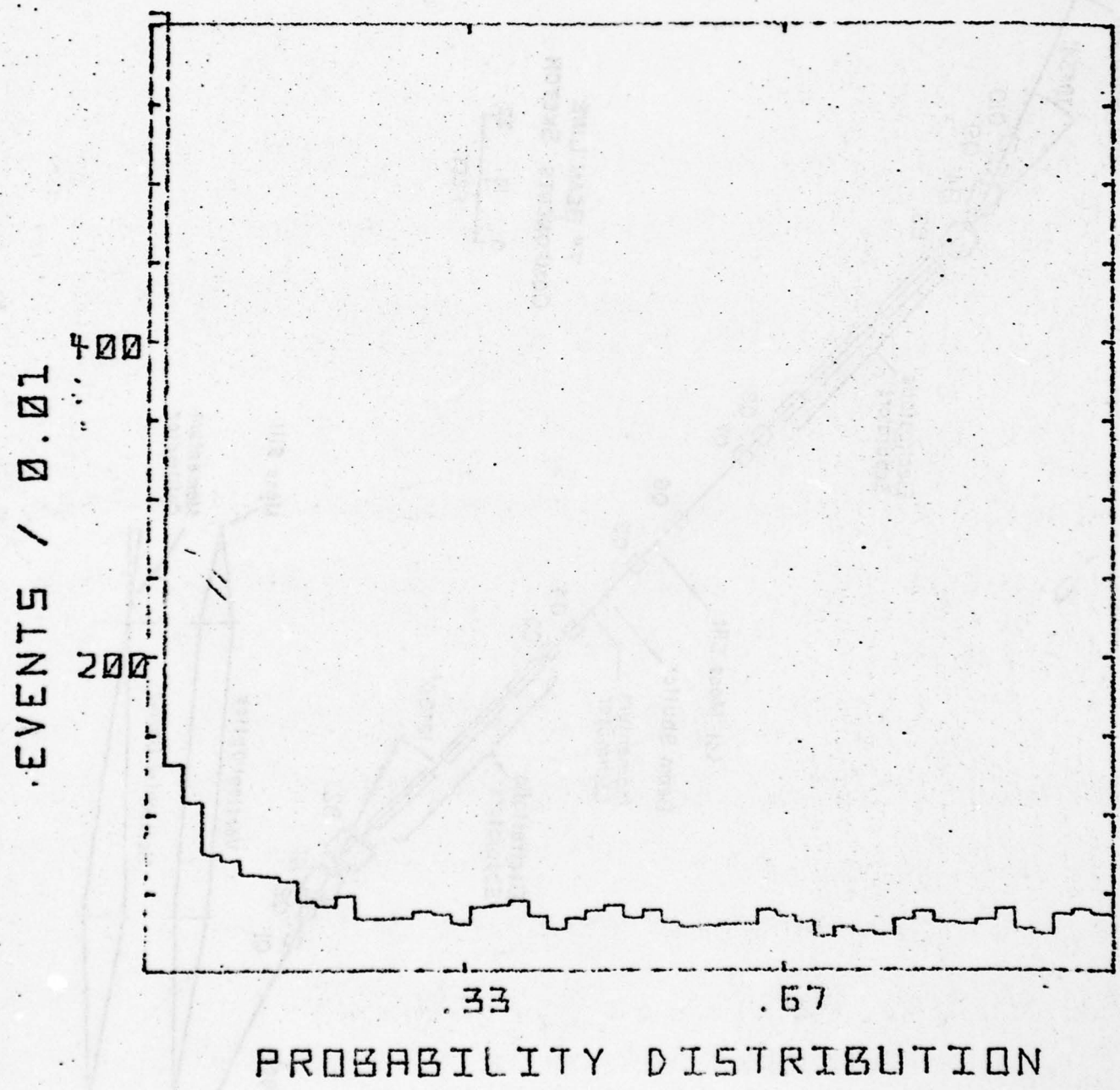

FIGURE 2

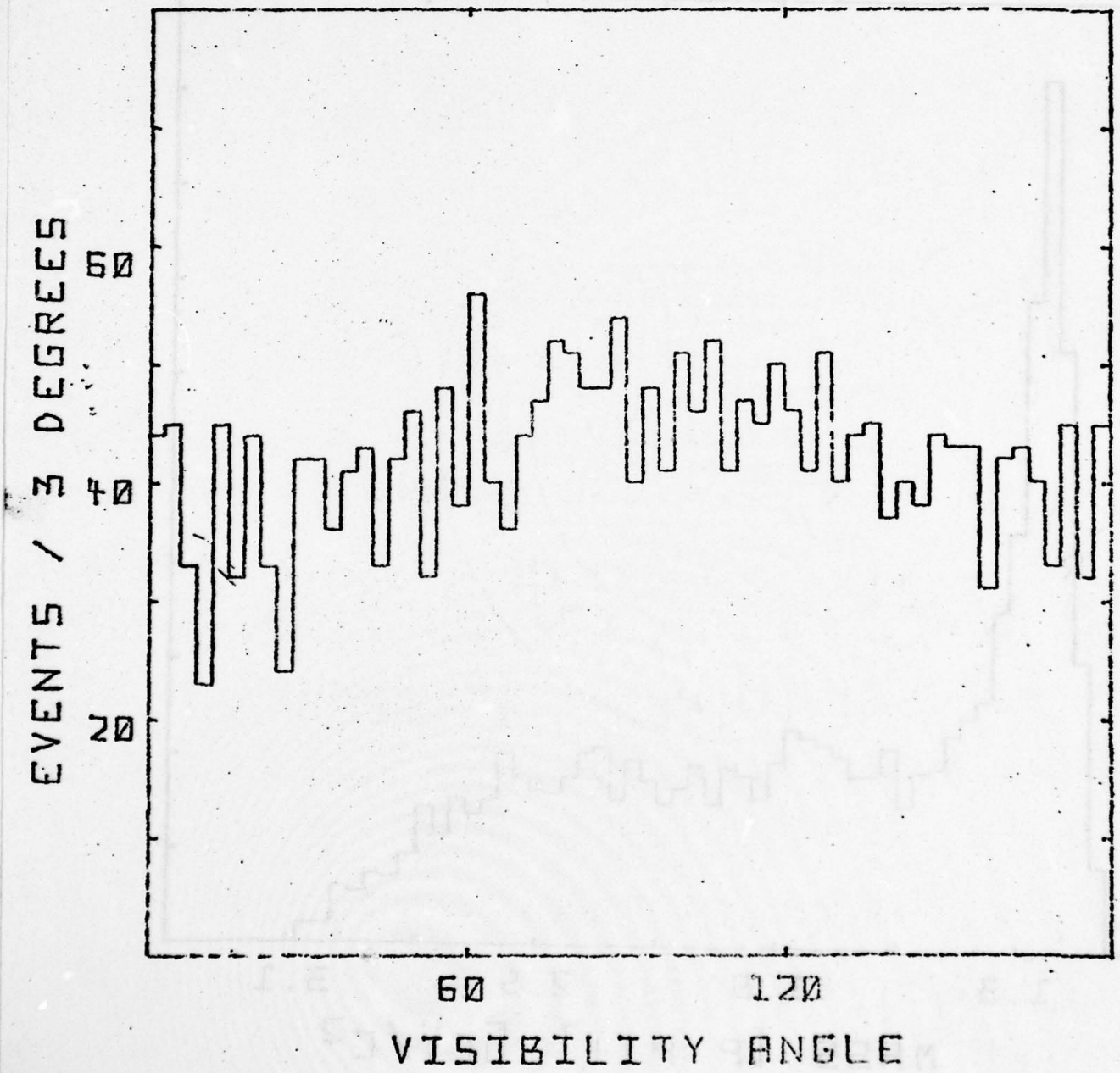

FIGURE 3

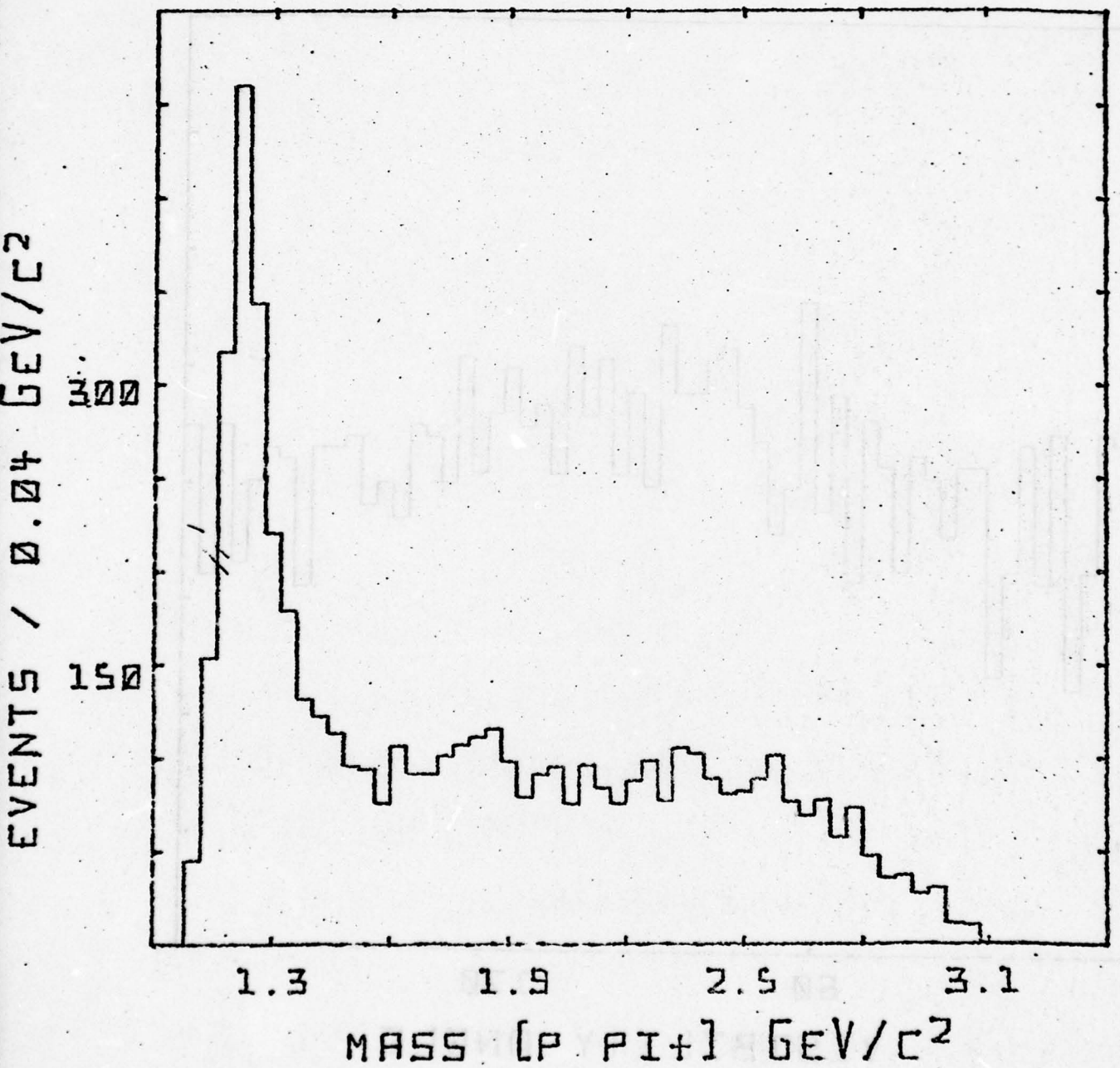

FIGURE 4

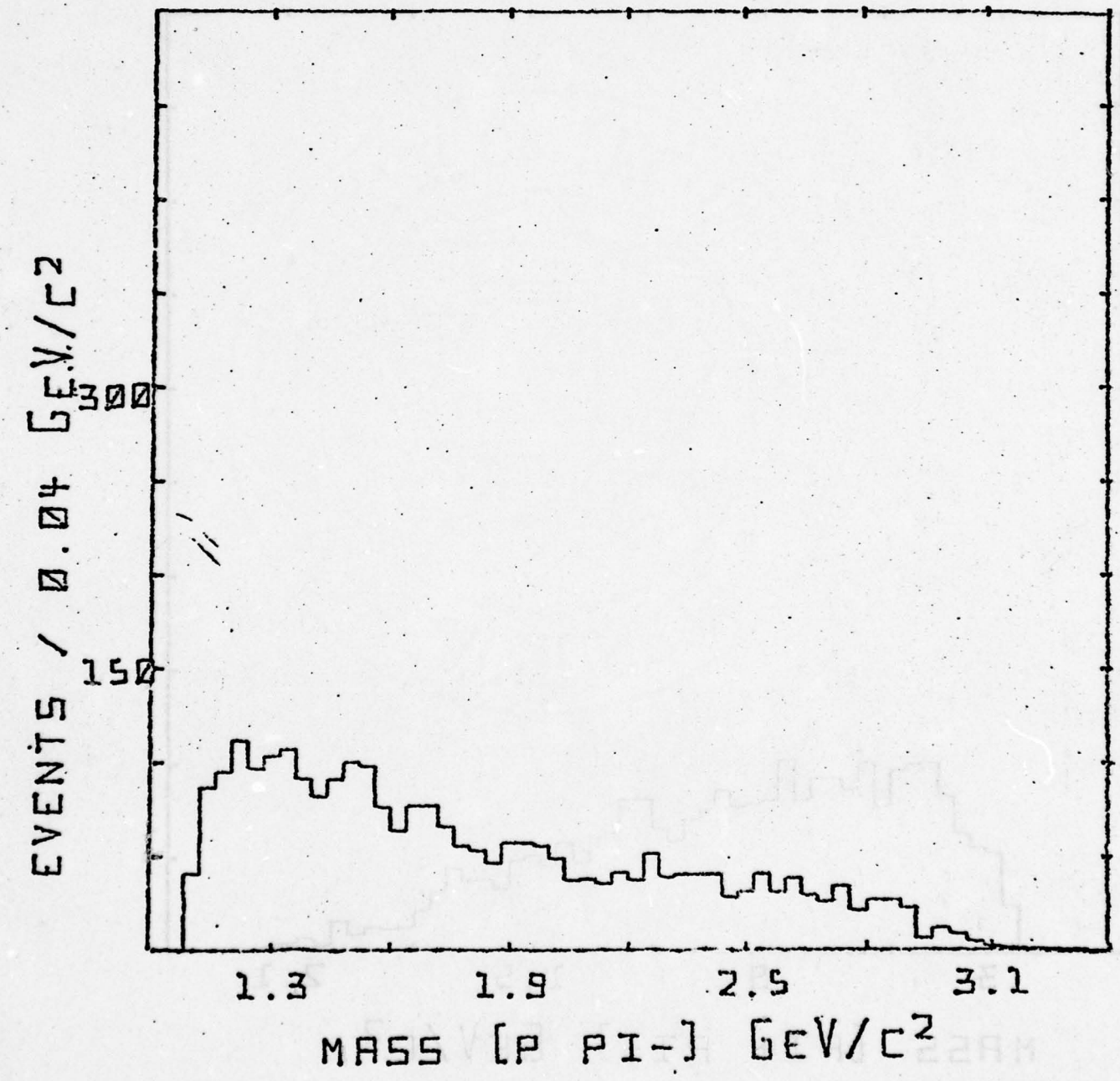

FIGURE 5

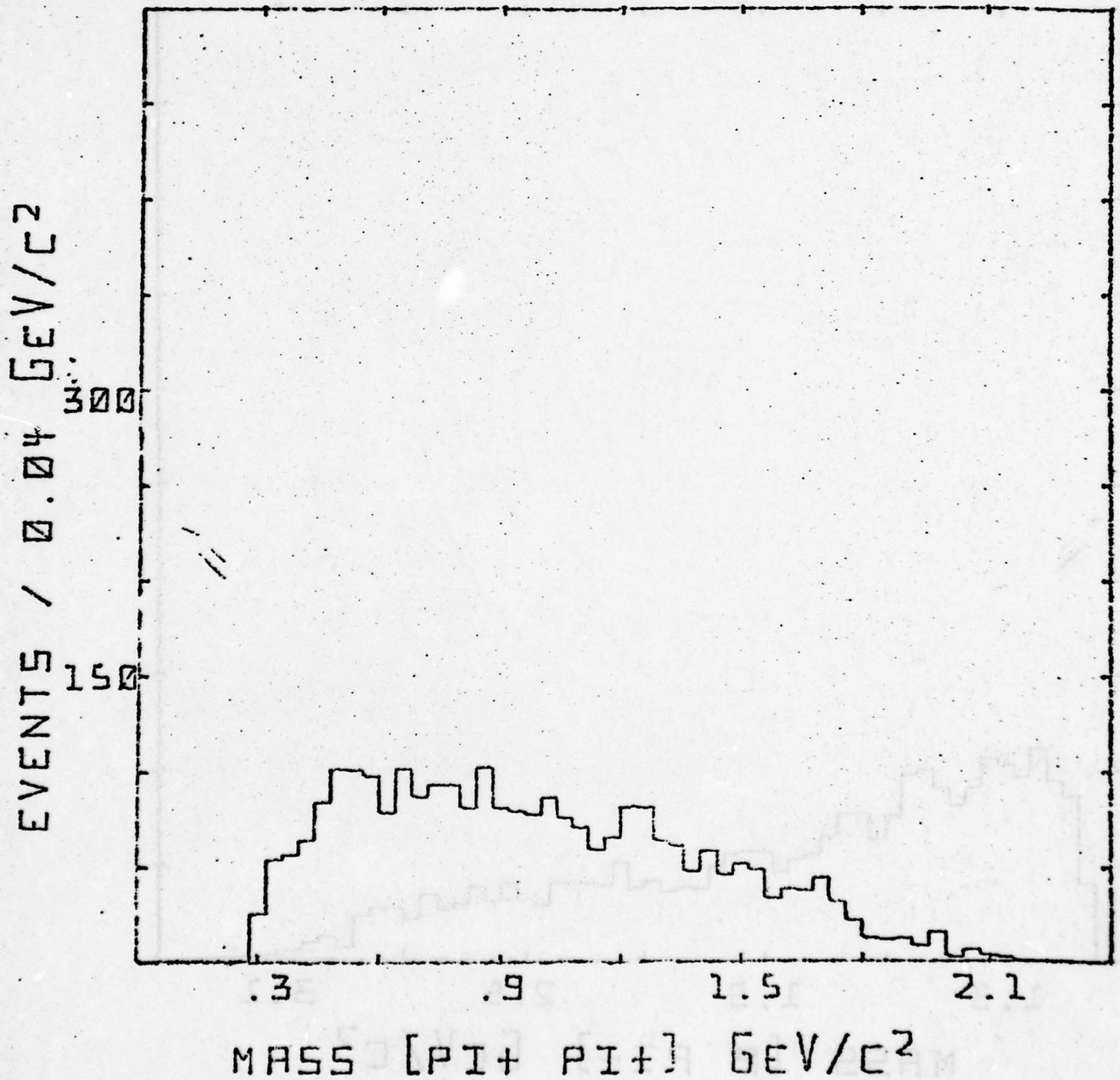

FIGURE 6

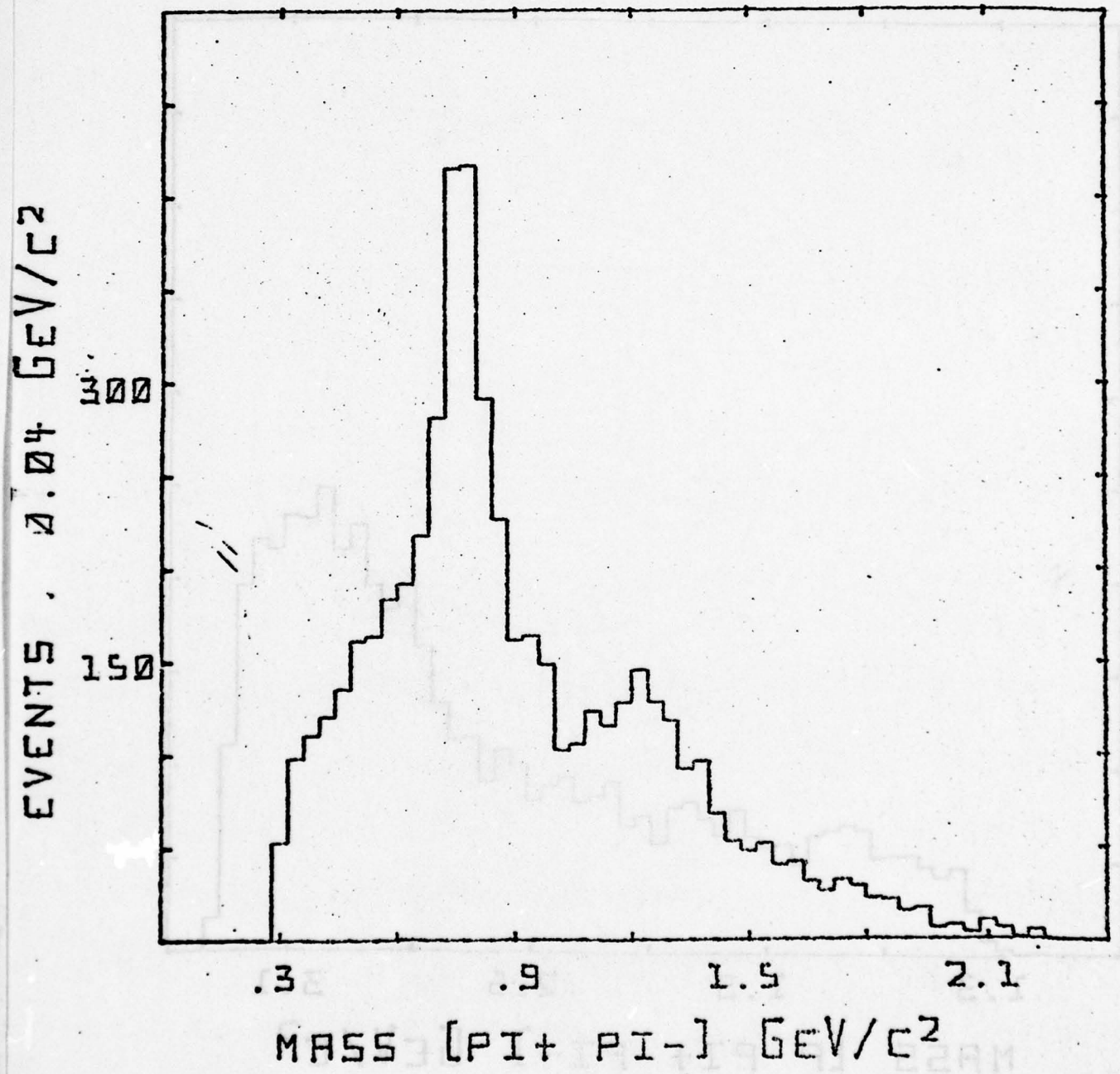

FIGURE 7

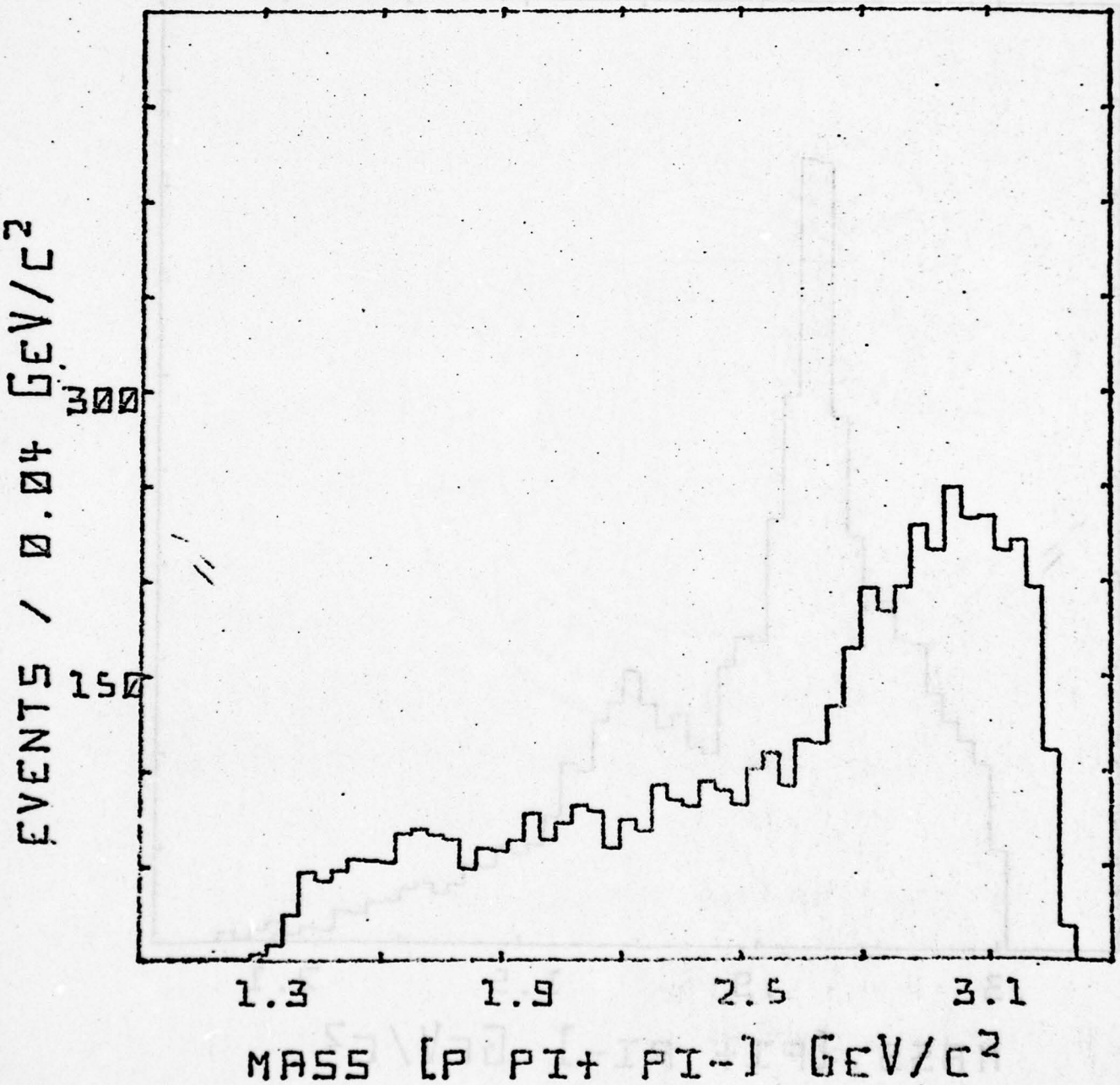

FIGURE 8

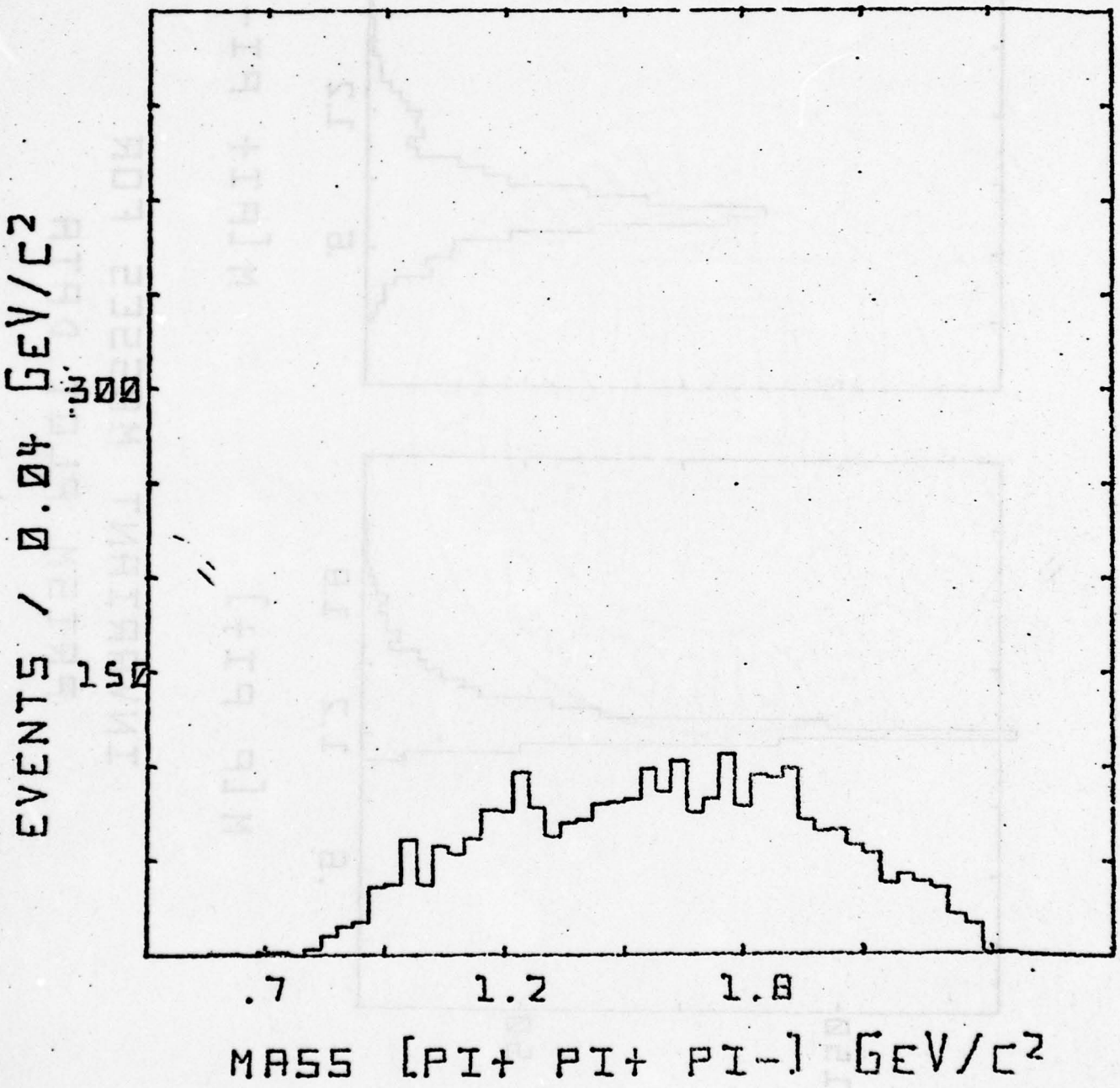

FIGURE 9

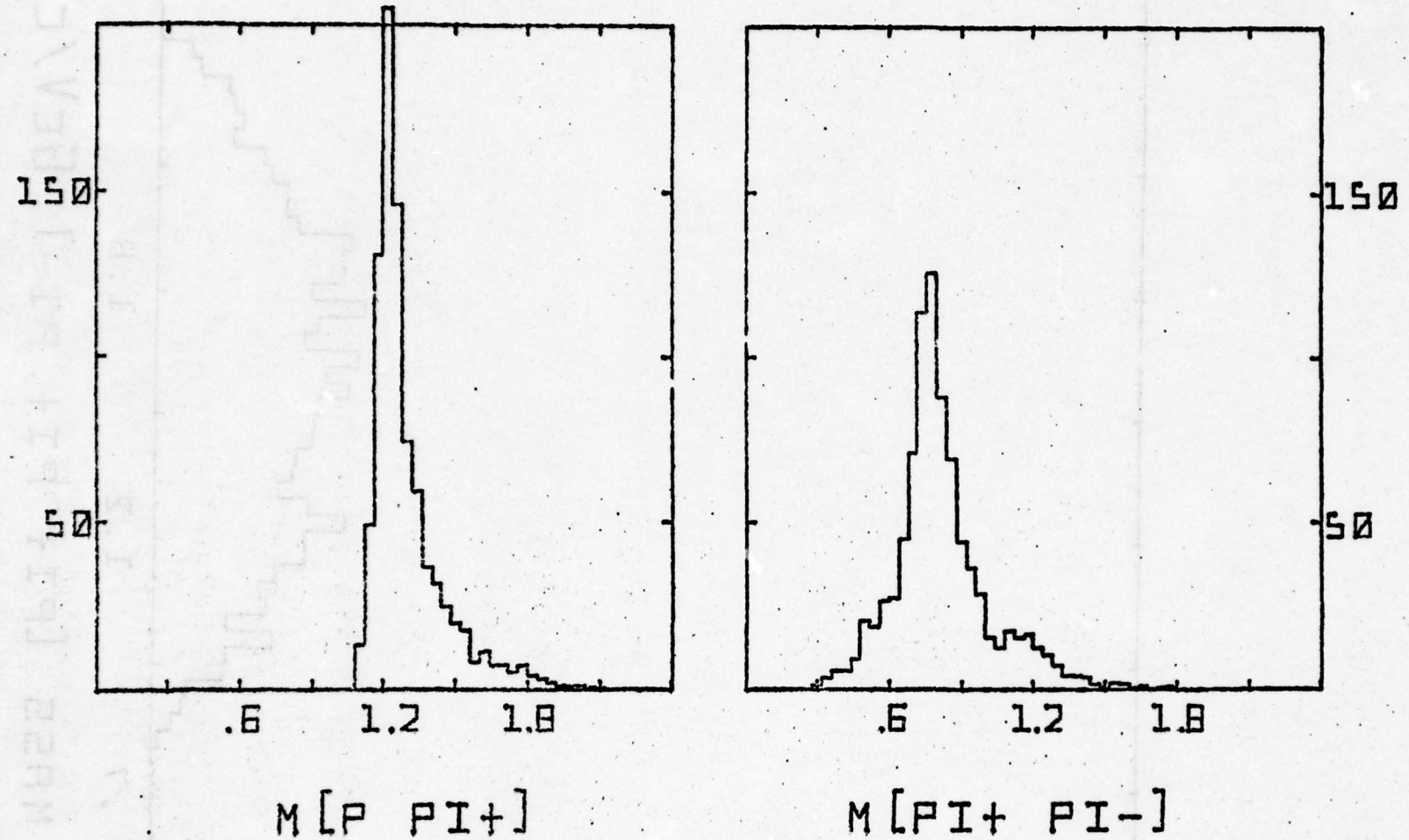

FIGURE 10

INVARIANT MASSES FOR
PRISM PLOT DATA

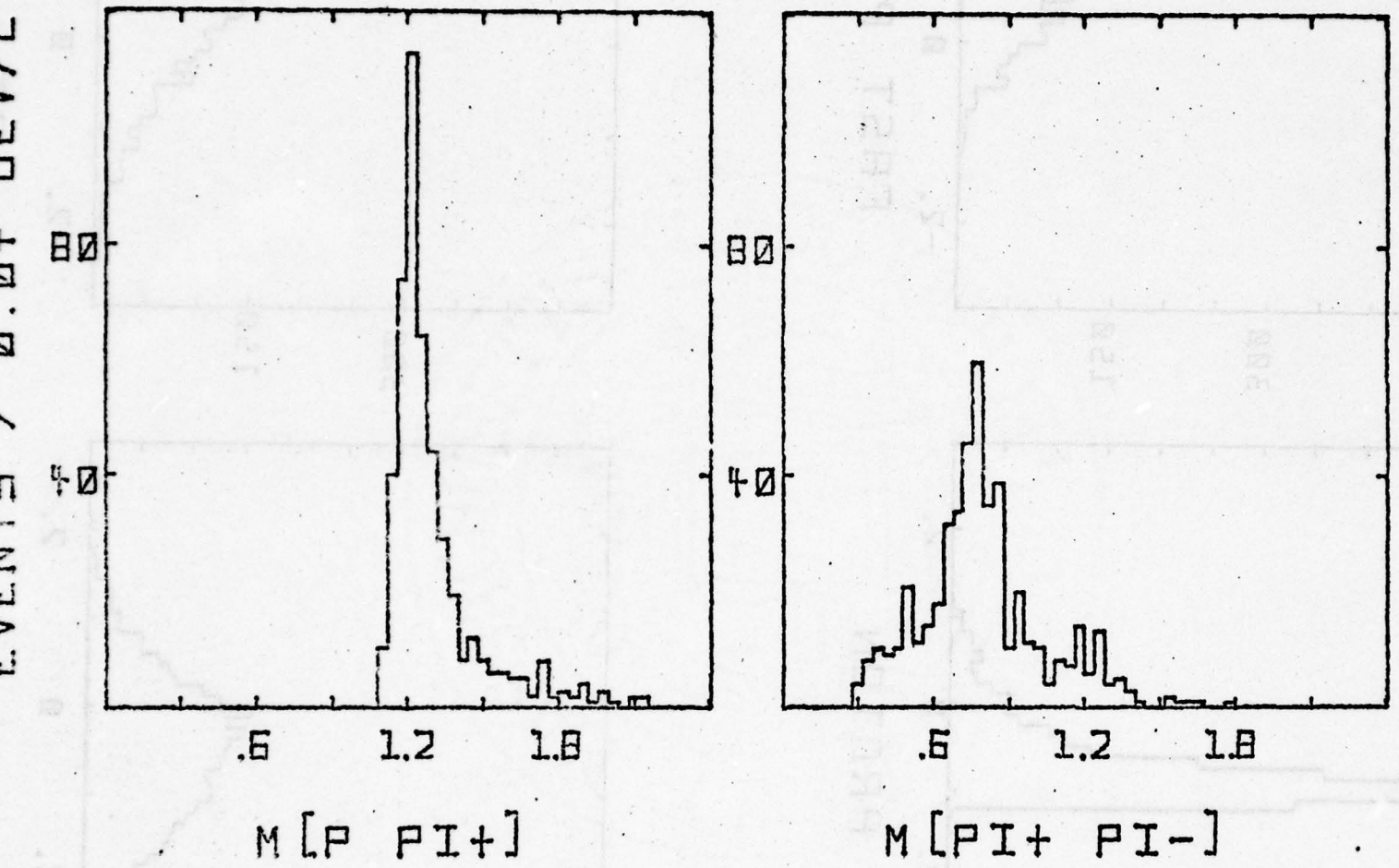

FIGURE 11

INVARIANT MASSES FOR
2X2 CLUSTERS

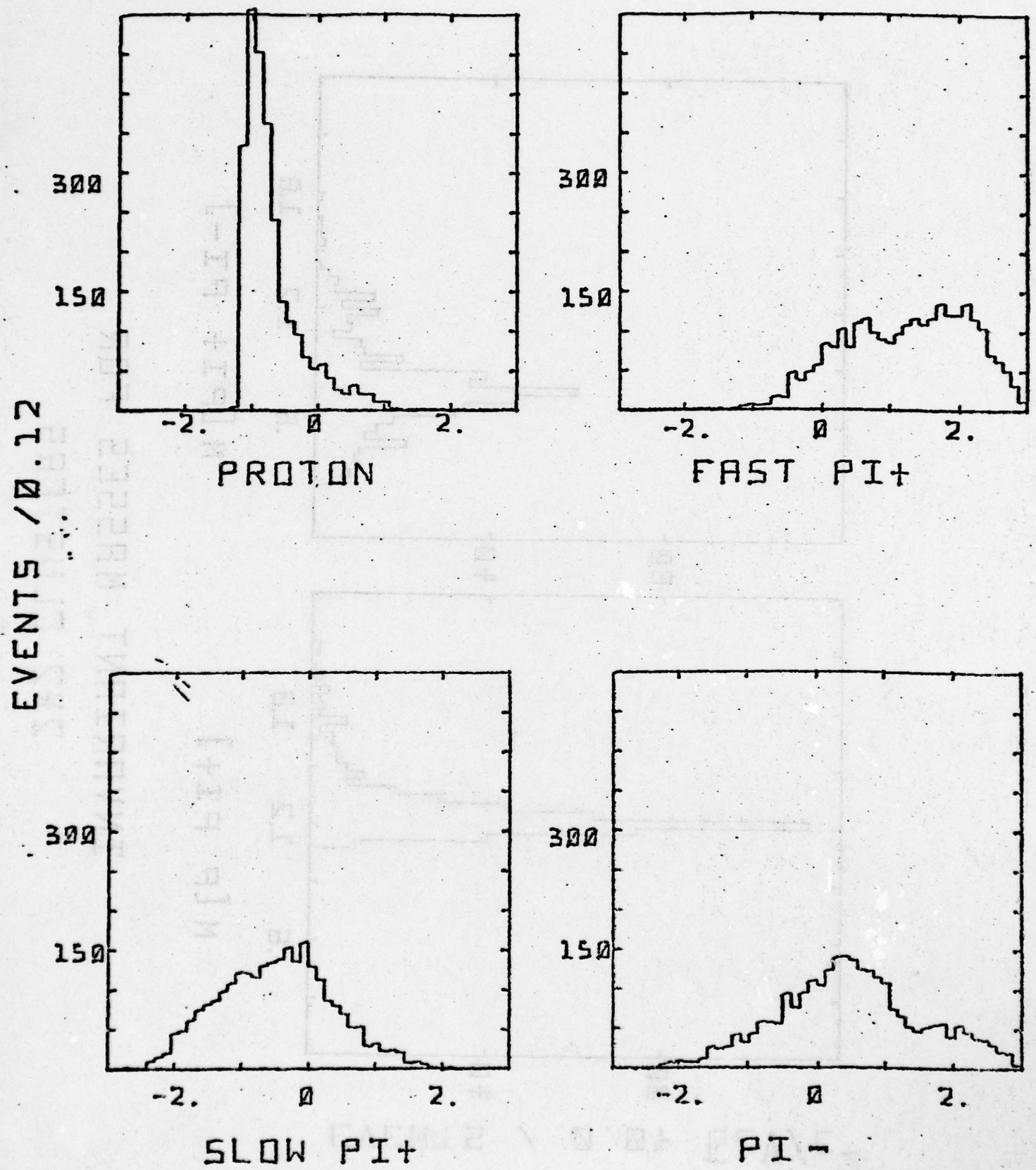
EVENTS /0.12
300
150
-2.
0
2.
PROTON
FAST PI+
SLOW PI+
PI-
RAPIDITY DISTRIBUTIONS

FIGURE 12

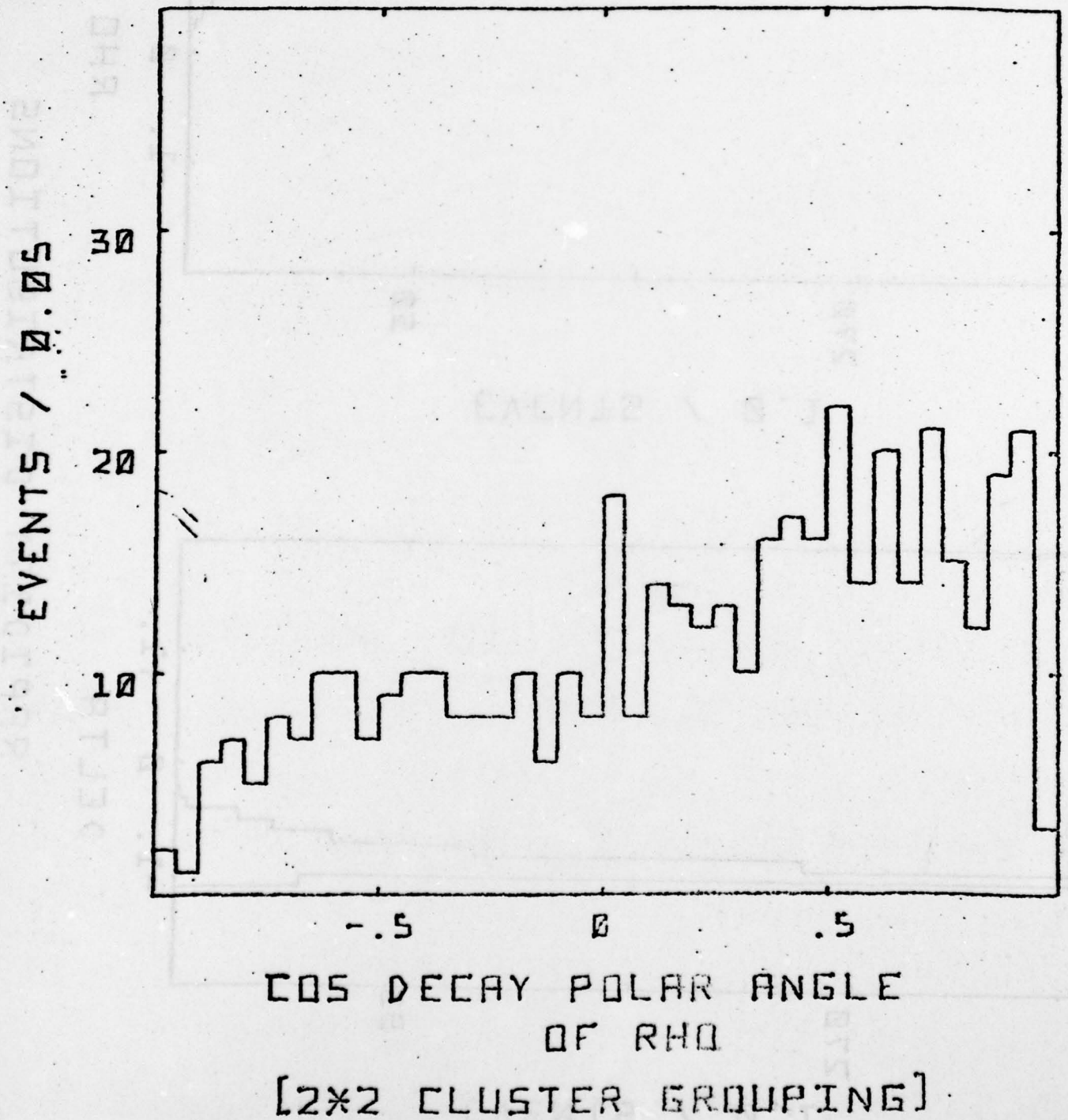
EVENTS / 0.05
30
20
10
-.5
0
.5
COS DECAY POLAR ANGLE
OF RHO
[2*2 CLUSTER GROUPING]

FIGURE 13

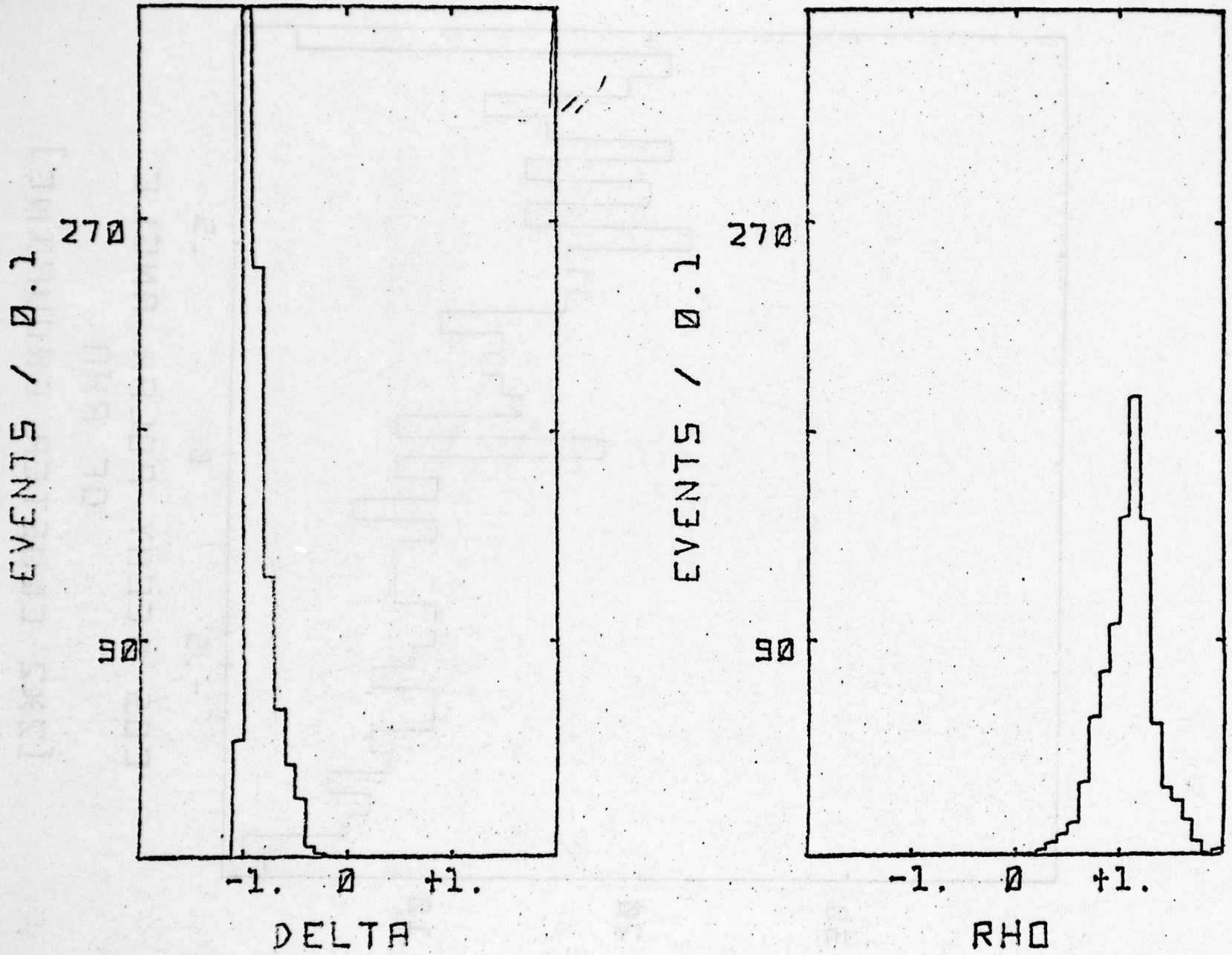

FIGURE 14

RAPIDITY DISTRIBUTIONS

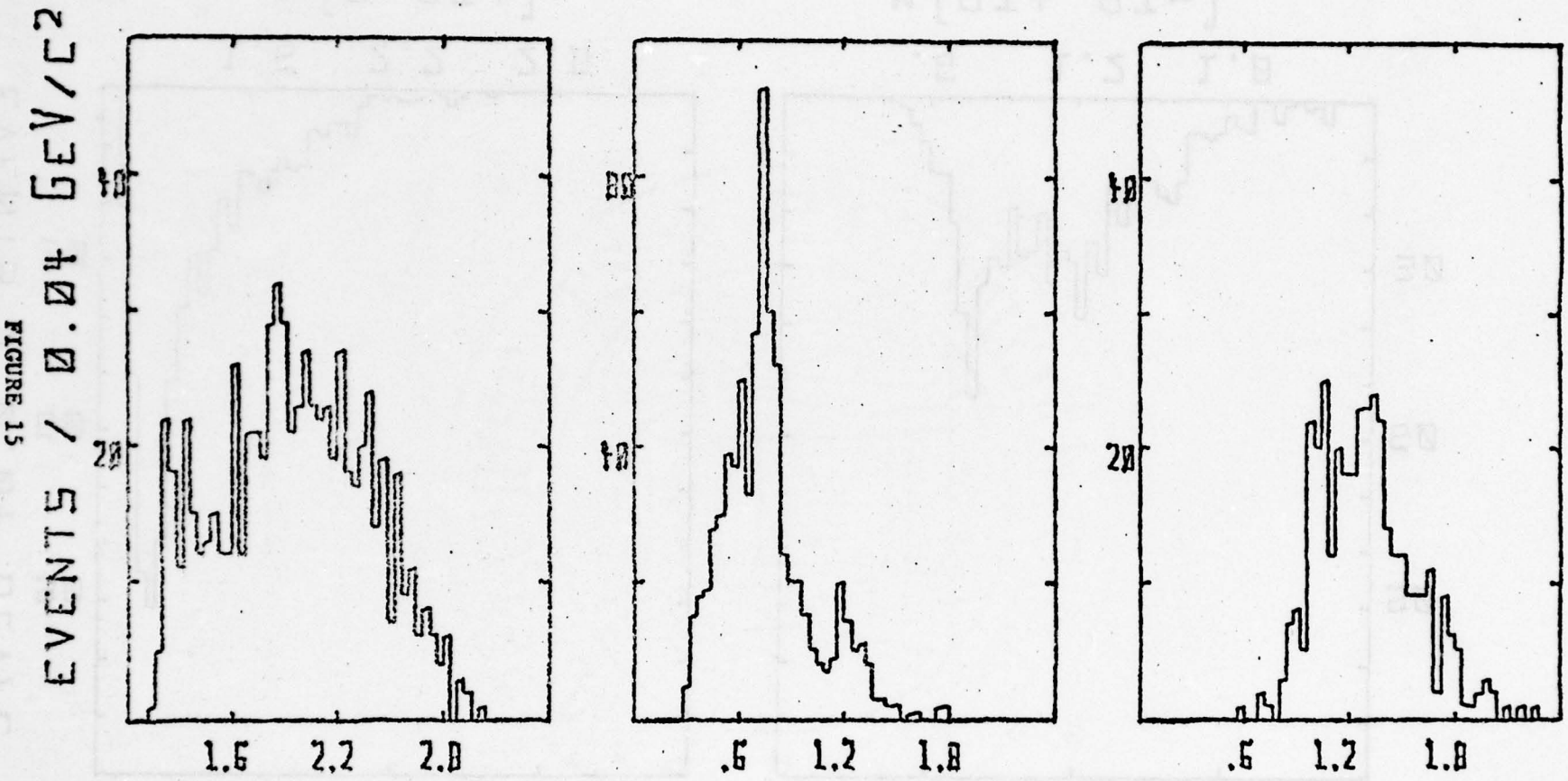

FIGURE 15

INVARIANT MASS PLOTS W/ P ALONE

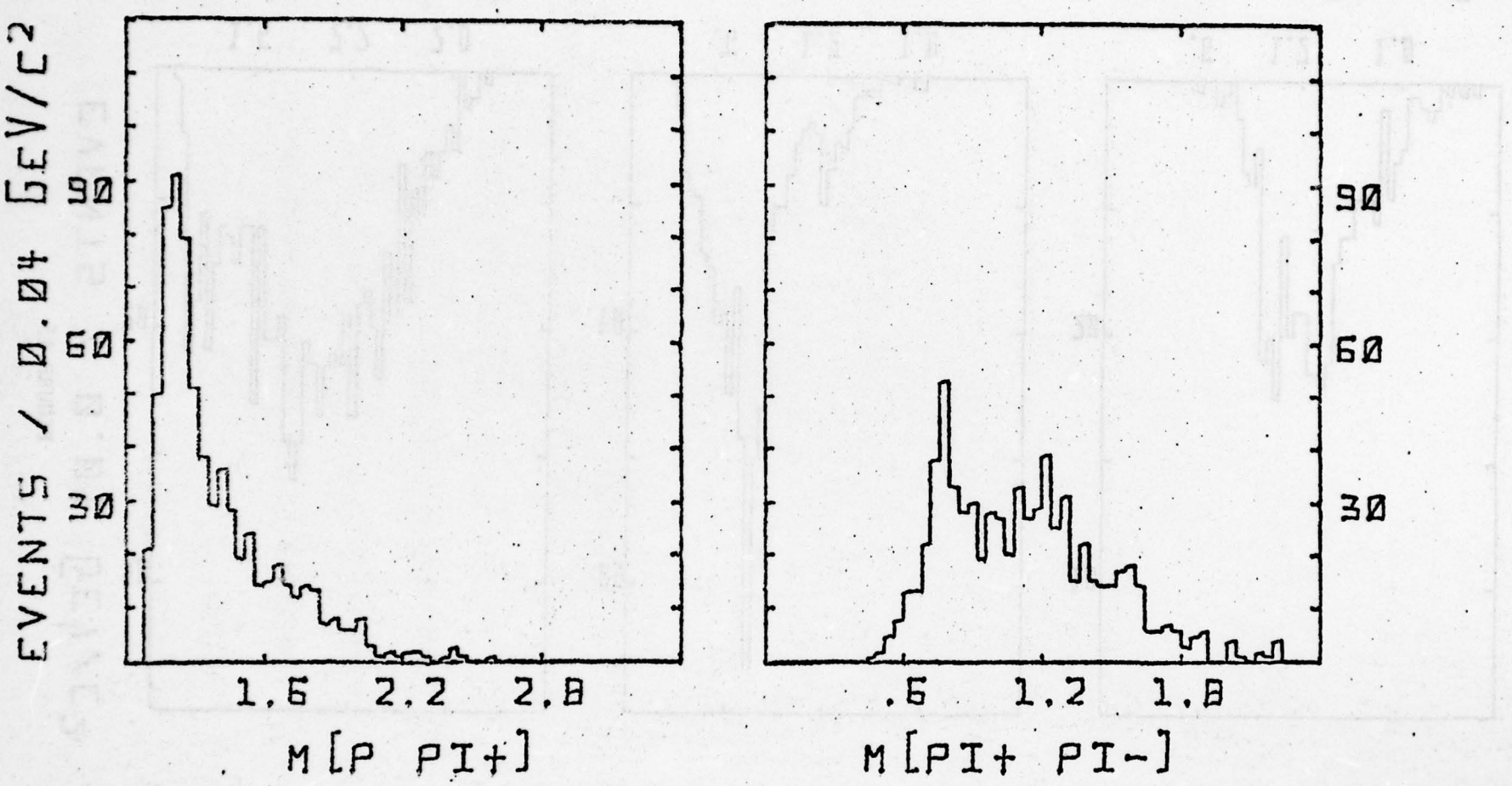

FIGURE 16

MASS PLOTS FOR
PI- ALONE CLUSTERS

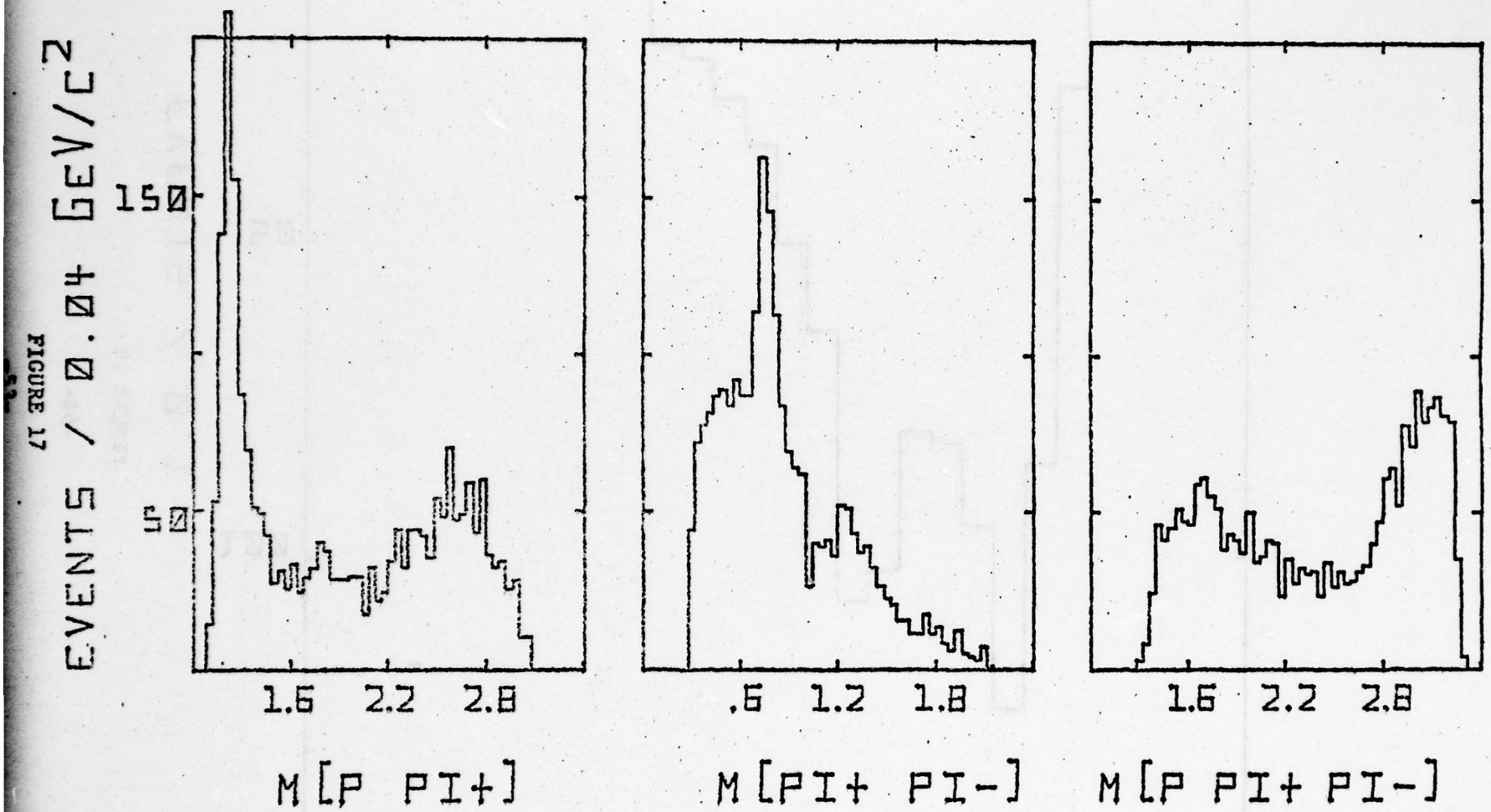

FIGURE 17

INVARIANT MASS PLOTS W/ PI+ ALONE

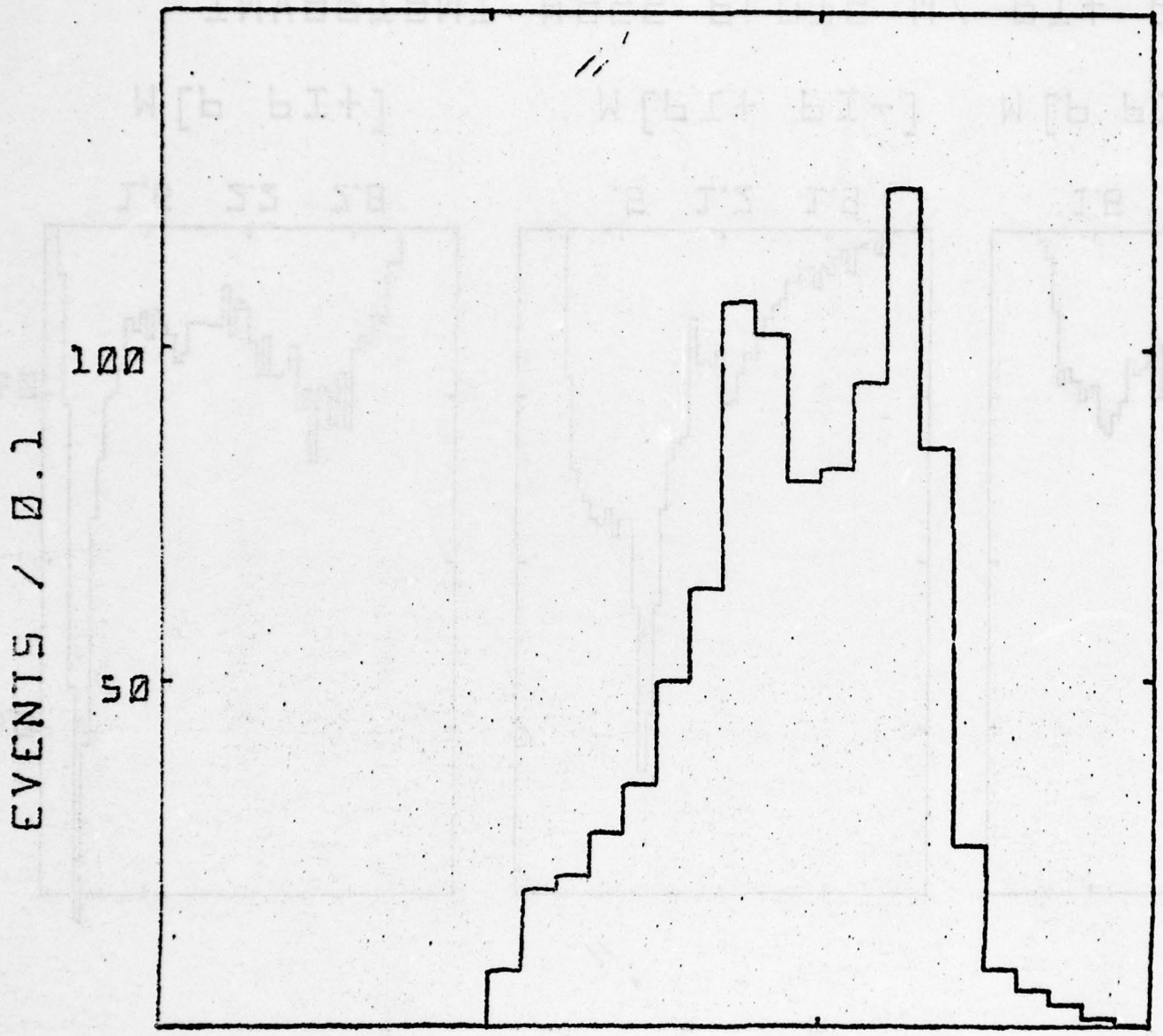
EVENTS / 0.1
100
50
0.
1.
RAPIDITY OF PI+PI- SYSTEM
FOR PI- ALONE CLUSTERS

FIGURE 18

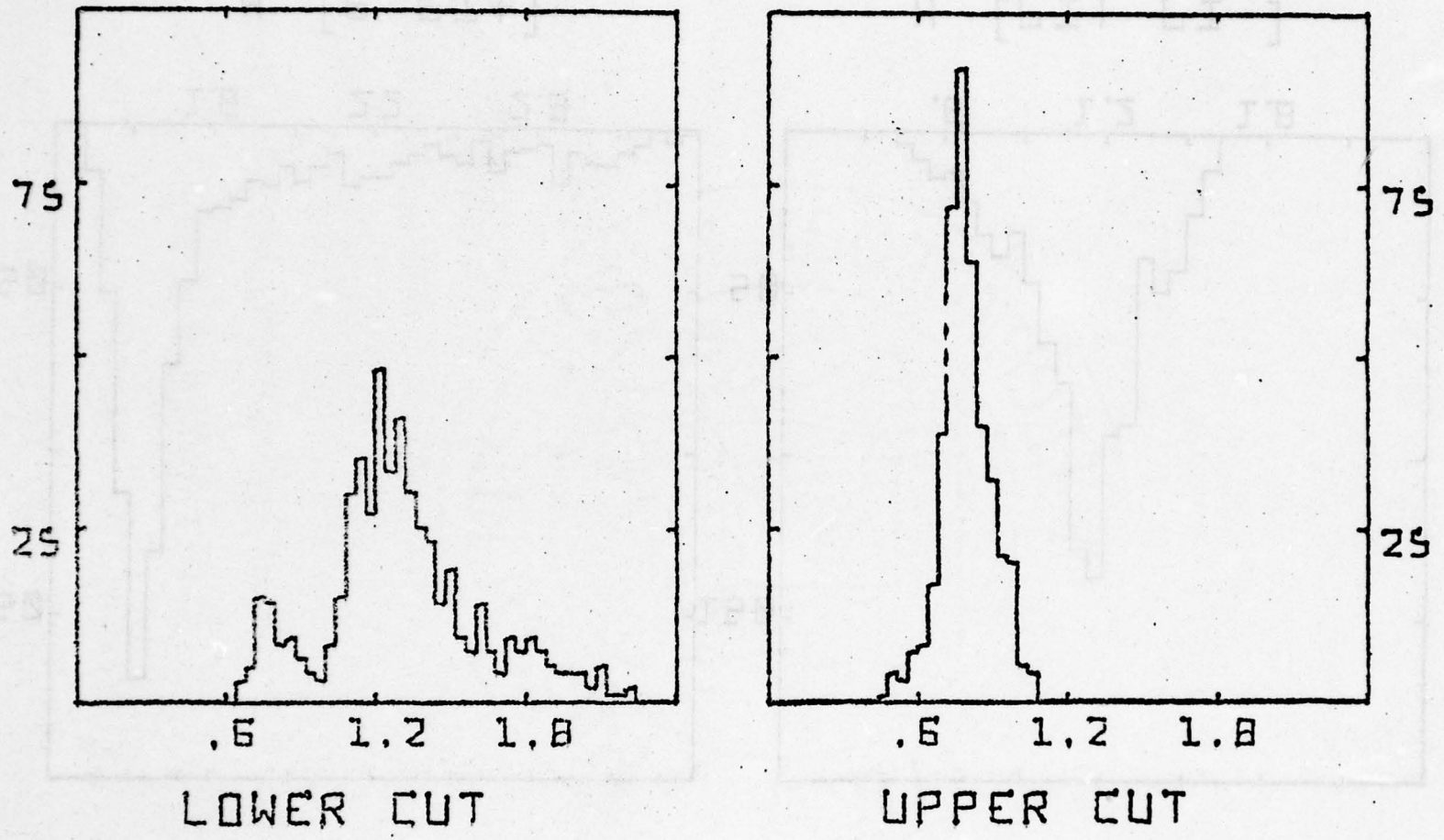
EVENTS / 0.04 GeV/C²
75
25
.6
1.2
1.8
LOWER CUT
75
25
.6
1.2
1.8
UPPER CUT
MASS [PI+ PI-]
AFTER RAPIDITY CUT

FIGURE 19

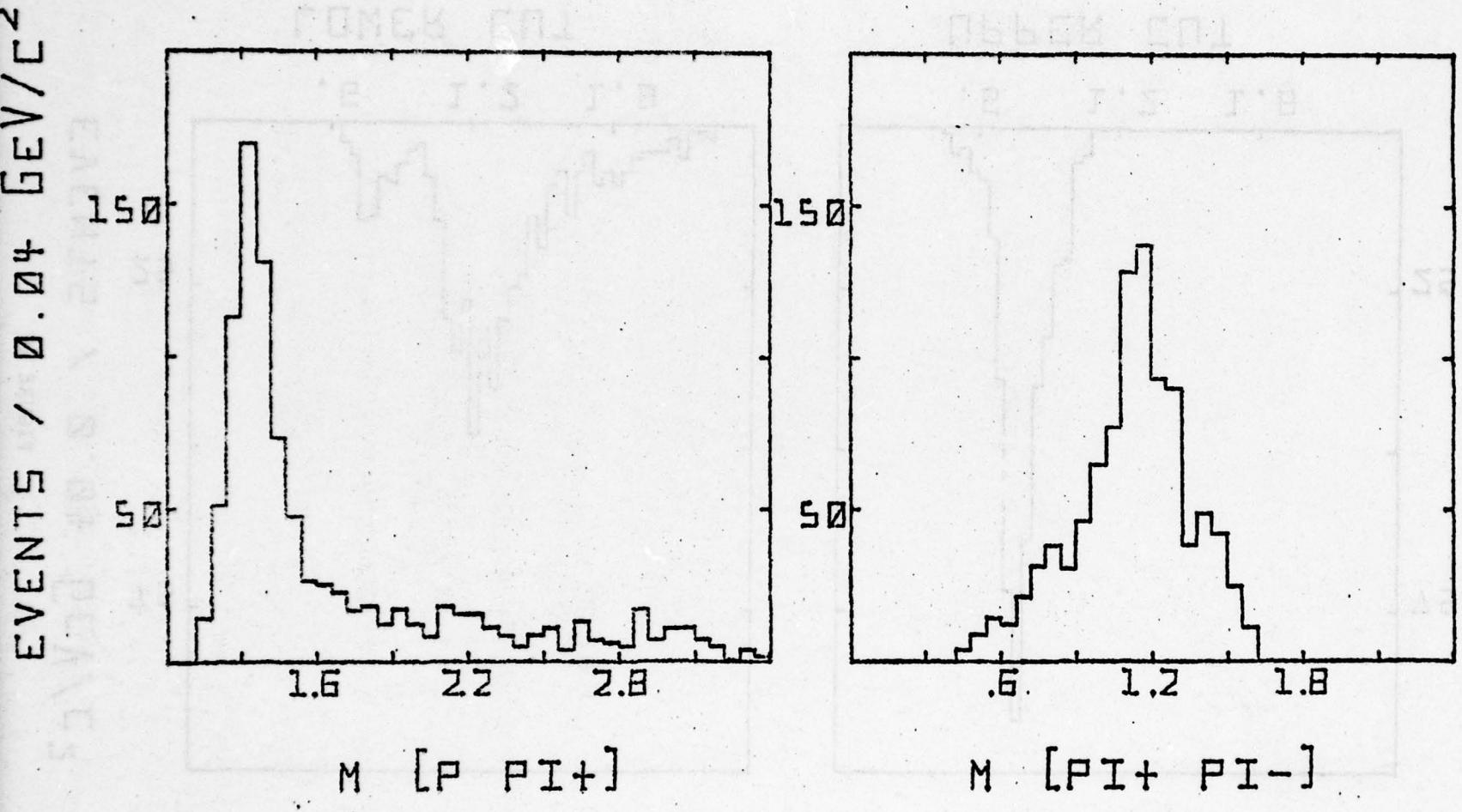

MASS DISTRIBUTIONS
CLUSTERED EVENTS

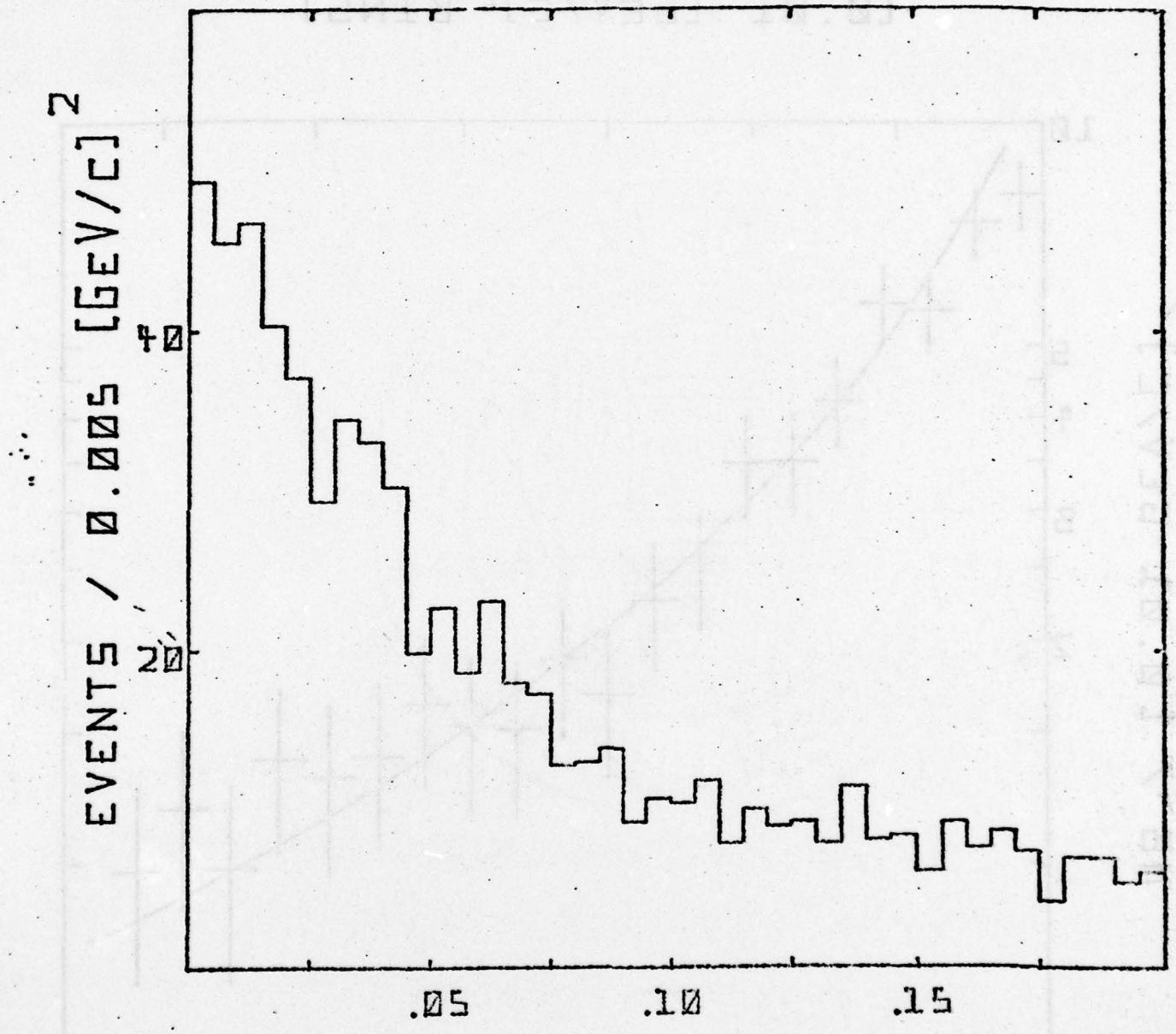

DIFF. CROSS SECTION FOR
PRISM PLOT DATA

FIGURE 21

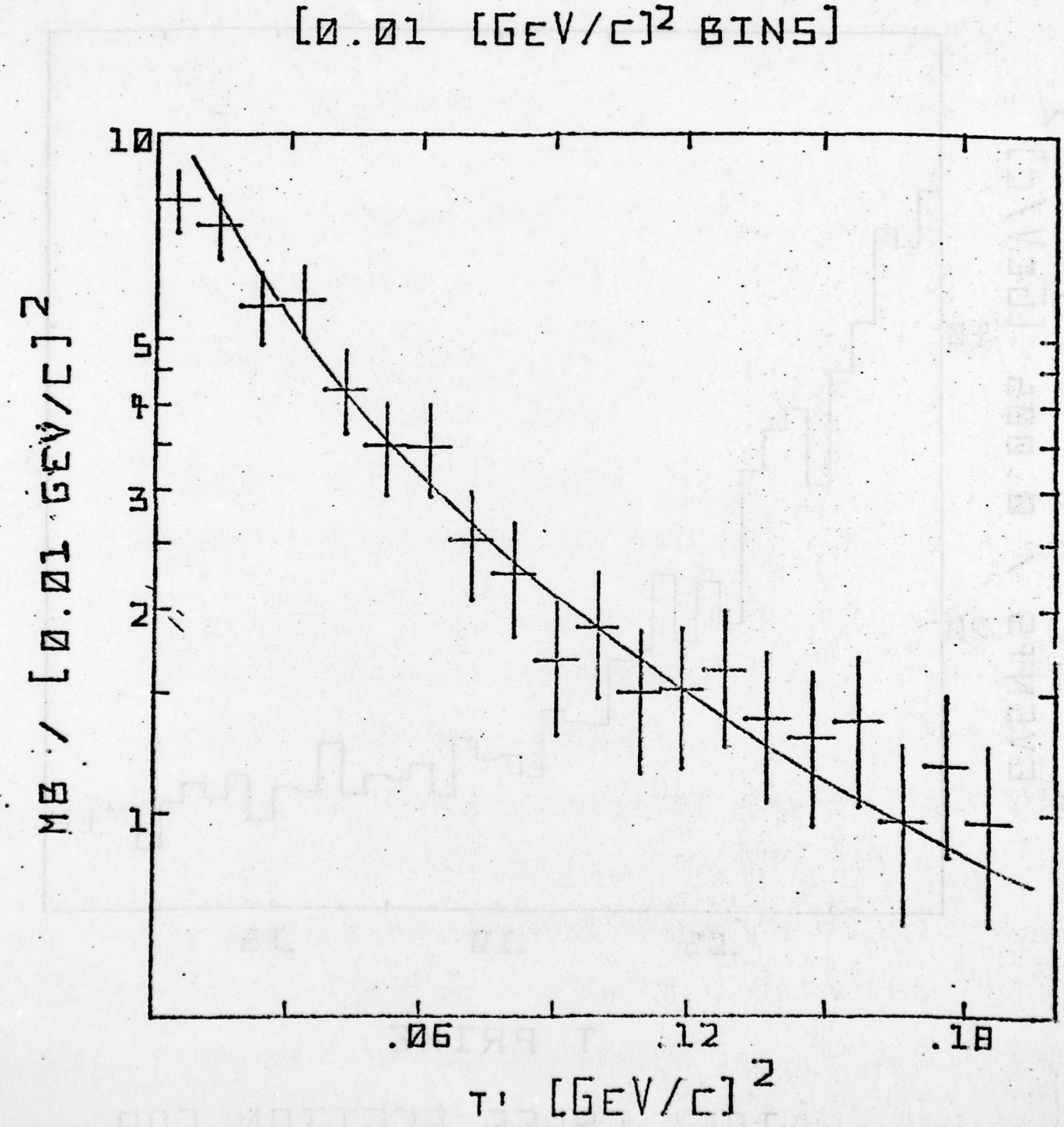

DIFF. CROSS SECTION

FIGURE 22

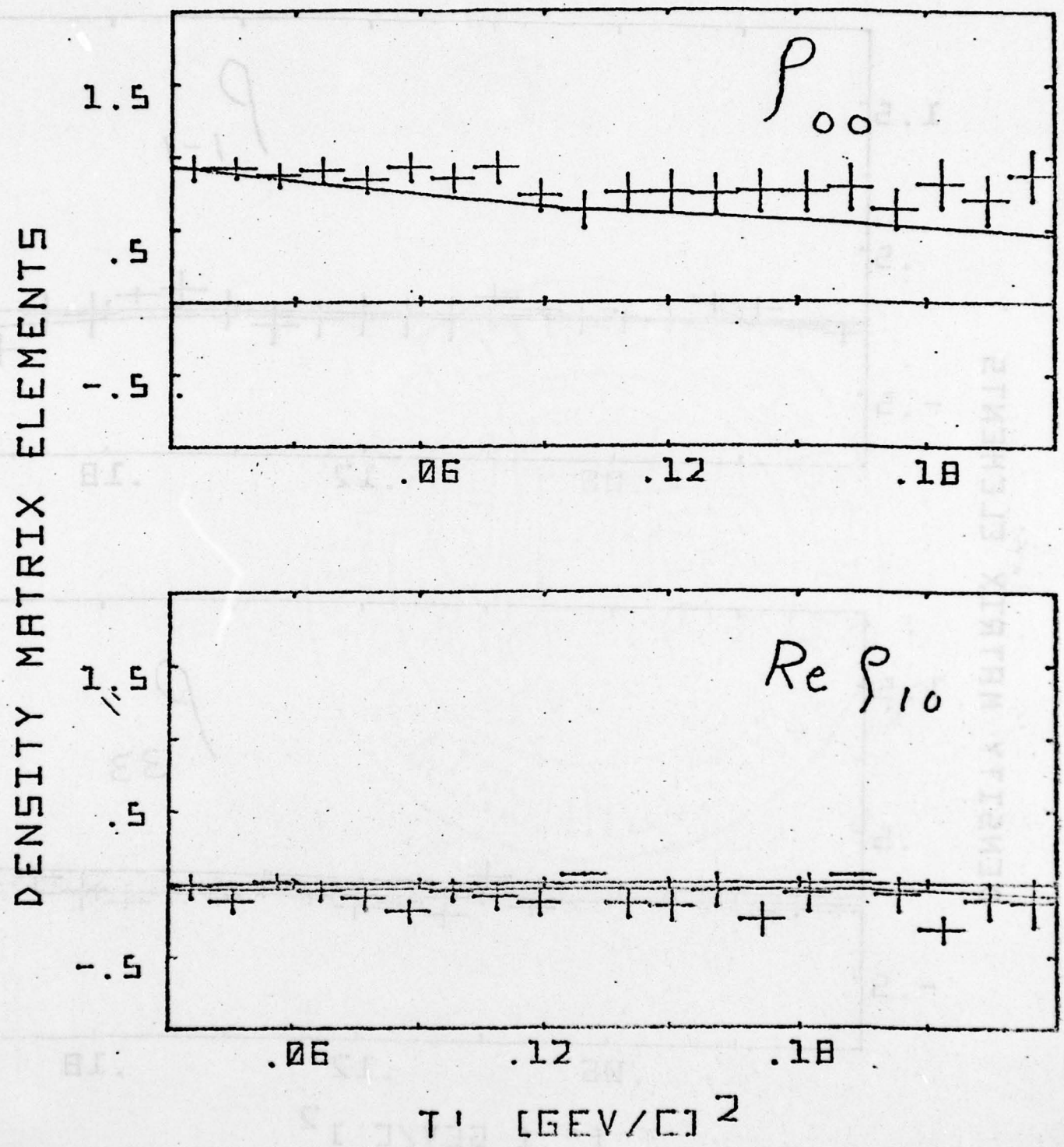
DENSITY MATRIX ELEMENTS
1.5
.5
-.5
.06
.12
.18
ρ_{00}
1.5
.5
-.5
.06
.12
.18
$Re\,\rho_{10}$
T' [GEV/C]^2

FIGURE 23

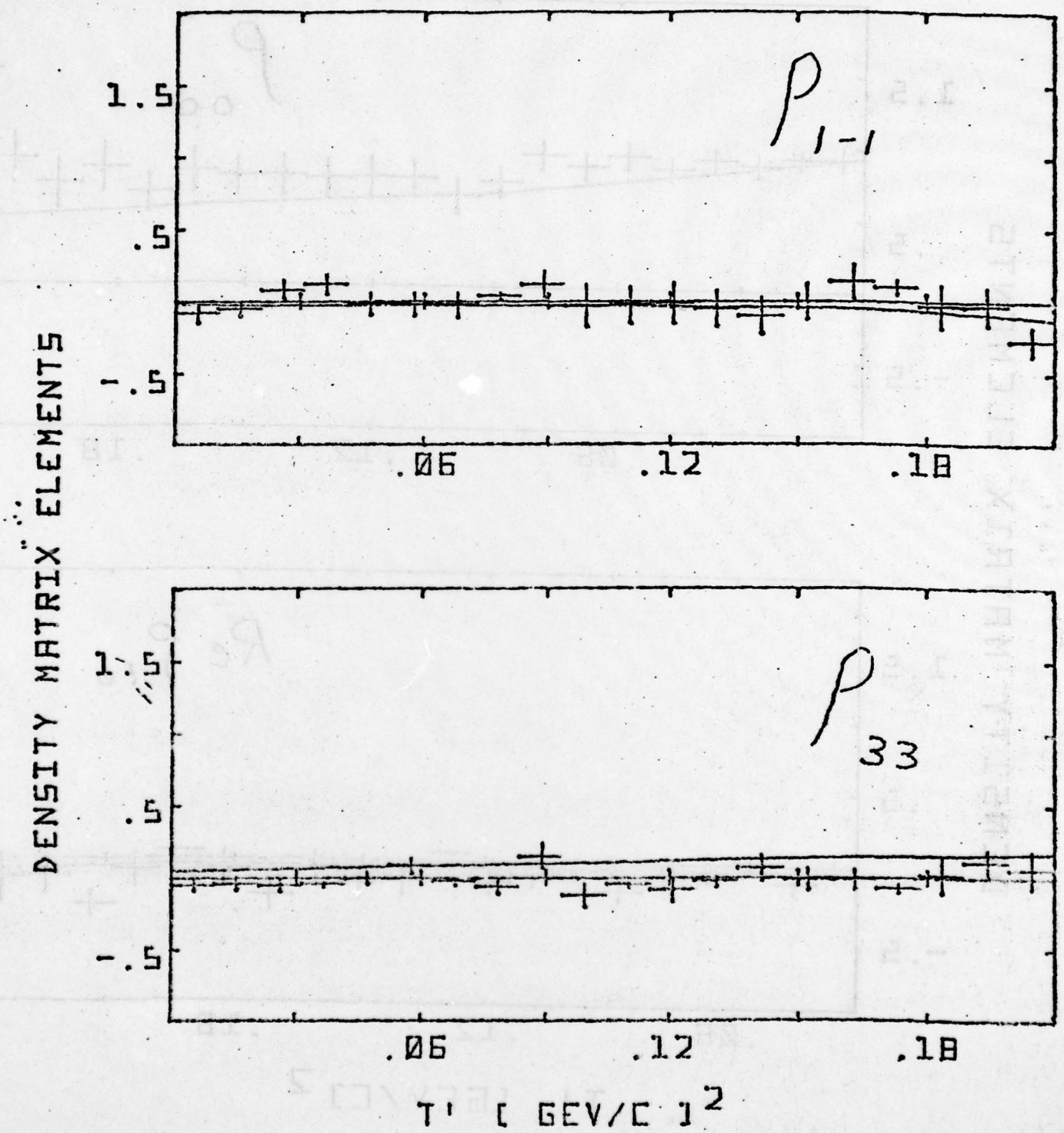
DENSITY MATRIX ELEMENTS
1.5
.5
-.5
ρ_{1-1}
.06
.12
.18
1.5
.5
-.5
ρ_{33}
.06
.12
.18
T' [GEV/C]^2

FIGURE 24

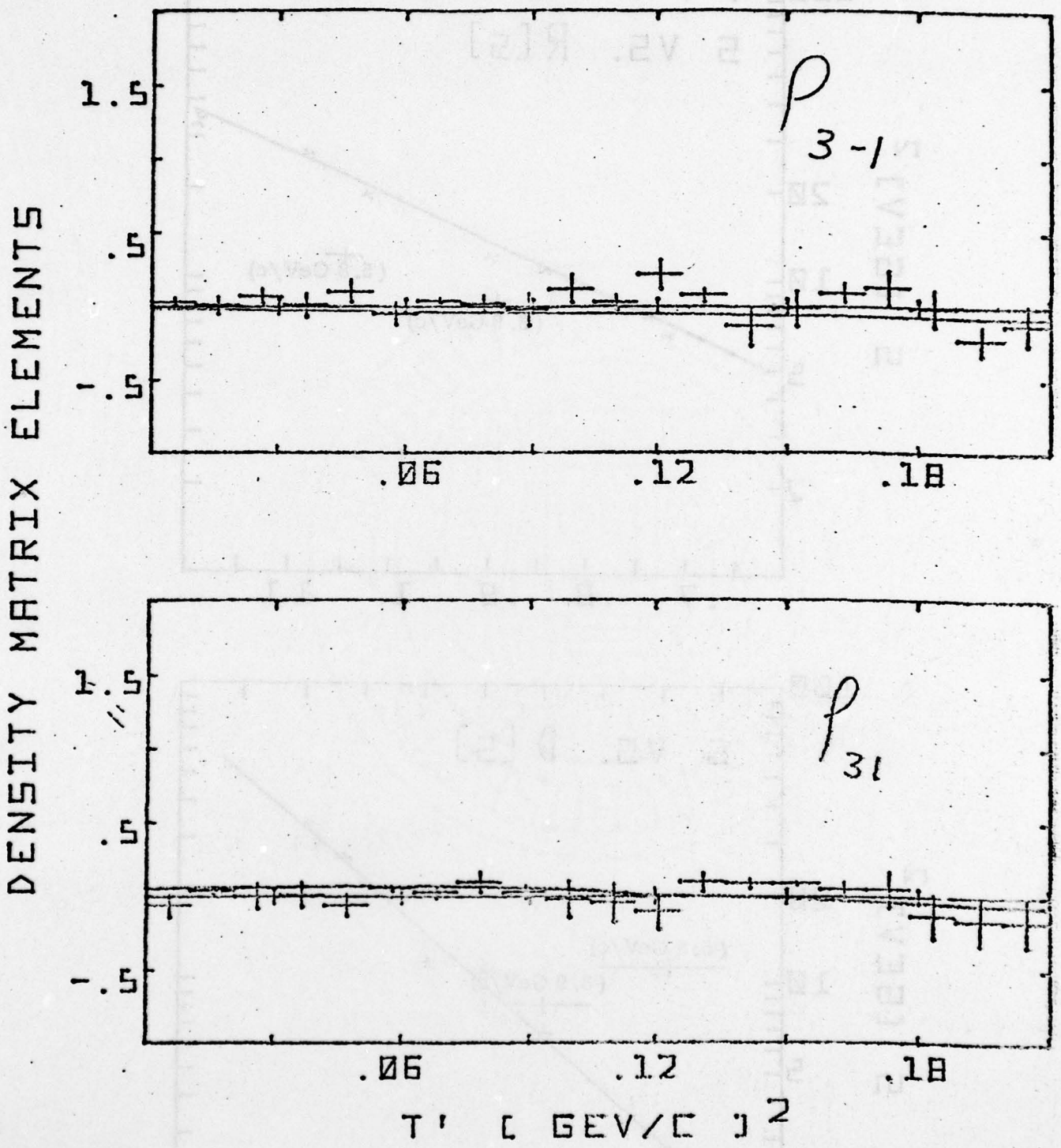
DENSITY MATRIX ELEMENTS
1.5
.5
-.5
.06
.12
.18
ρ_{3-1}
1.5
.5
-.5
.06
.12
.18
ρ_{31}
T' [GEV/C]^2

FIGURE 25

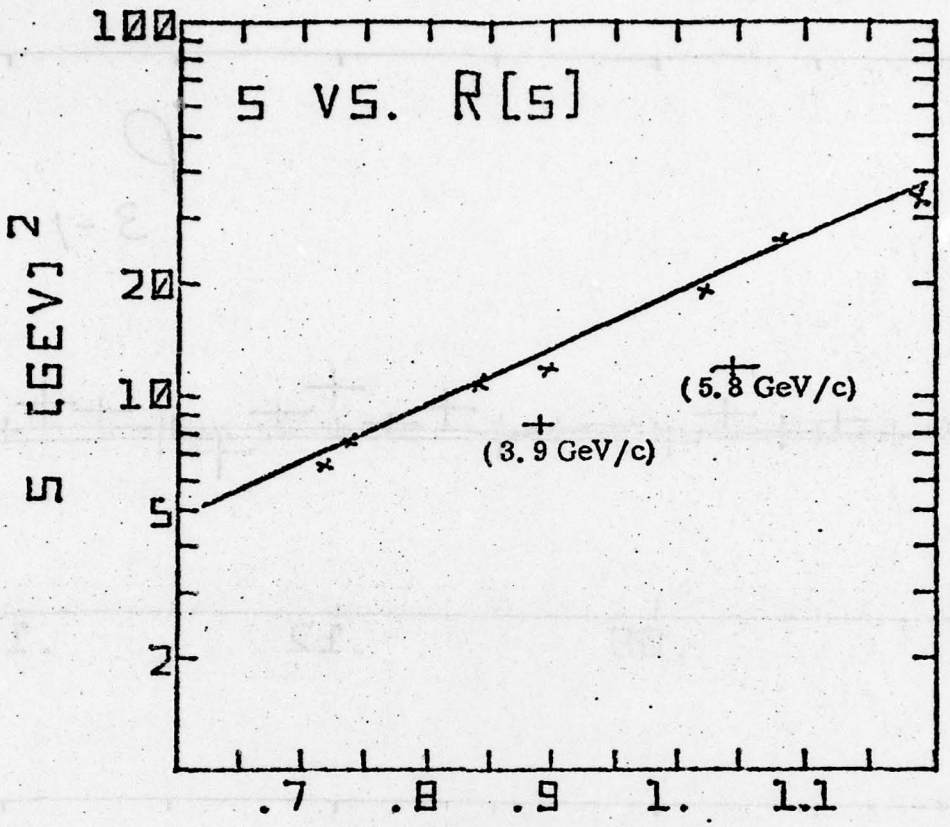
S VS. R[S]
S [GEV] 2
100
20
10
5
2
.7
.8
.9
1.
1.1
(5.8 GeV/c)
(3.9 GeV/c)

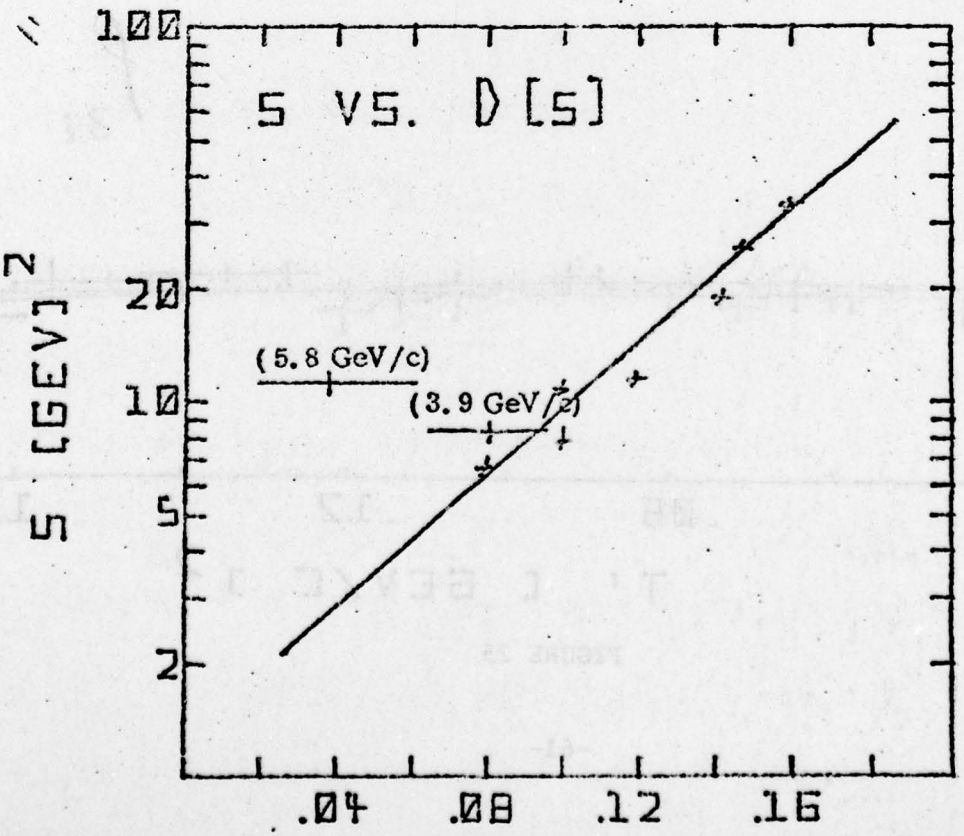
S VS. D[S]
S [GEV] 2
100
20
10
5
2
.04
.08
.12
.16
(5.8 GeV/c)
(3.9 GeV/c)

FIGURE 26